A MULTIDISCIPLINARY INVESTIGATION OF THE INTERMEDIATE DEPTHS OF THE ATLANTIC OCEAN: AAIW $\delta^{13}C$ VARIABILITY DURING THE YOUNGER DRYAS AND LITHOHERMS IN THE STRAITS OF FLORIDA

A Dissertation

by

BRIAN NEVILLE BROOKSHIRE JR.

Submitted to the Office of Graduate Studies of
Texas A&M University
in partial fulfillment of the requirements for the degree of

DOCTOR OF PHILOSOPHY

December 2010

Major Subject: Oceanography

A Multidisciplinary Investigation of the Intermediate Depths of the Atlantic Ocean: AAIW $\delta^{13}C$ Variability During the Younger Dryas and Lithoherms in the Straits of Florida

A MULTIDISCIPLINARY INVESTIGATION OF THE INTERMEDIATE DEPTHS OF THE ATLANTIC OCEAN: AAIW $\delta^{13}C$ VARIABILITY DURING THE YOUNGER DRYAS AND LITHOHERMS IN THE STRAITS OF FLORIDA

A Dissertation

by

BRIAN NEVILLE BROOKSHIRE JR.

Submitted to the Office of Graduate Studies of
Texas A&M University
in partial fulfillment of the requirements for the degree of

DOCTOR OF PHILOSOPHY

Approved by:

Chair of Committee,	Niall C. Slowey
Committee Members,	Jack G. Baldauf
	Mitchell J. Malone
	Deborah J. Thomas
Head of Department,	Piers Chapman

December 2010

Major Subject: Oceanography

ABSTRACT

A Multidisciplinary Investigation of the Intermediate Depths of the Atlantic Ocean: AAIW $\delta^{13}C$ Variability During the Younger Dryas and Lithoherms in the Straits of Florida. (December 2010)

Brian Neville Brookshire Jr., B.S., Eckerd College; M.S., Texas A&M University

Chair of Advisory Committee: Dr. Niall C. Slowey

A transect of cores ranging from 798 m to 1585 m water depth in the South Atlantic Ocean document the relative intermediate water mass nutrient geometry and stable isotopic variability of AAIW during the Younger Dryas cooling event. The data reveal concurrent $\delta^{13}C$ and $\delta^{18}O$ excursions of 0.59 $^{0}/_{00}$ and 0.37 $^{0}/_{00}$ within the core of Antarctic Intermediate Water (AAIW) centered at 11,381 calendar years before present based on radiometric age control. A portion of the $\delta^{13}C$ variability (0.22 $^{0}/_{00}$) can be explained by a shift in thermodynamic equilibrium concurrent with a drop in temperature of 1.8°C at the locus of AAIW formation. The remaining 0.37 $^{0}/_{00}$ increase in $\delta^{13}C$ most likely resulted from increased wind velocities, and a greater coupling between the ocean and the atmosphere at the locus of AAIW formation (increased efficiency of the thermodynamic process).

Deepwater coral mounds are aggregates of corals, other organisms, their skeletal remains, and sediments that occur on the seafloor of the world's oceans. In the Straits of Florida, these features have been referred to as lithoherms. We use digital, side-scan

sonar data collected from the submarine NR-1 from an 10.9 km^2 area at ~650 m water depth to characterize quantitatively aspects of the morphology of 216. Their lengths, widths, heights, areas, orientations and concentration on the seafloor have been determined. Analysis indicates that the outlines of relatively small to medium sized lithoherms can be effectively described with a piriform function. This shape is less applicable to the largest lithoherms because they are aggregates of smaller lithoherms. Nearly all of the lithoherms studied have axes parallel to the northward flowing Florida Current, and the heads of 80% of these features face into the current. The shape and orientation of the lithoherms, and evidence of megaripples and scouring in the sonar data suggest that these features are formed by a unidirectional current.

Following an extensive investigation of over 200 lithoherms via side-scan sonar imagery and direct observation, we have developed a qualitative model for the formation of the lithoherm type of deep-water coral mounds in the Straits of Florida. Lithoherm formation can be characterized by four main stages of development: nucleating, juvenile, mature singular, and fused. Fused lithoherms can form via transverse and/or longitudinal accretion, however, transverse accretion at the head of the mound is likely the most efficient mechanism. A comparison of lithoherm spatial relationship to local bathymetry agrees with previous observations of deep-water coral mound formations along the levied margins of density flow scour channels.

ACKNOWLEDGEMENTS

I would like to thank Niall Slowey for serving as my committee chair and providing multiple avenues of research during my time at Texas A&M. Niall's devotion to the science of oceanography will always be an inspiration. I would also like to thank Jack Baldauf, Debbie Thomas and Mitch Malone for serving on my committee, and for providing much needed feedback during the course of my degree.

In addition, I would like to thank Mary Brookshire, Will Cain, Nick Collins and Sharath Ravula for their graciousness over the years in providing feedback and assistance. Thanks also to TDI-Brooks International for generously providing sedimentary materials essential to this research, and to the June 2002 crew of the submarine *NR-1* for assistance in geophysical data procurement. Finally, thanks to the National Science Foundation for supporting portions of this research.

TABLE OF CONTENTS

LIST OF FIGURES

FIGURE Page

LIST OF TABLES

CHAPTER I

INTRODUCTION AND GENERAL SIGNIFICANCE

The intermediate depths of the world's oceans (approximately 600 – 2000 m) are important for many reasons. Primarily, intermediate depth water masses control thermocline ventilation, and play a large role in oceanic carbon sequestration (Broecker and Peng 1982). Changes in intermediate water mass stable and radiogenic isotopic composition can be derived from geochemical signals in marine sedimentary sequences. These signals may then be evaluated in order to determine changes in the mode of intermediate water mass formation, circulation rate and geometry. Here, we present $\delta^{13}C$ and $\delta^{18}O$ evidence of intermediate water variability in the south Atlantic during the Younger Dryas cooling event. We offer a reasonable scenario to explain this variability, with specific importance placed on the role of Antarctic Intermediate Water (AAIW). This research represents new contribution to the relatively small pool of knowledge pertaining to intermediate water mass response to the Younger Dryas cooling event in the South Atlantic Ocean.

Another important aspect of intermediate ocean depths, are continental slope seafloor environments. In particular, deep-water coral reefs are found extensively along the southeast Atlantic coast of the United States at around 700 m depth (Reed et al. 2006).

This dissertation follows the style of the Journal of Sedimentary Research.

These deep-water reefs, here referred to as Lithoherms (Neumann et al. 1977), have largely been described in a qualitative fashion. In contrast to this, we present quantitative data on lithoherm morphology and distribution derived from high resolution (150kHz) side-scan sonar data collected from onboard the US Navy's NR-1 submarine. With perspective derived from the quantitative analysis of the side-scan sonar data and visual observations while made onboard the submarine, we also offer a qualitative model for lithoherm formation.

These two subjects have a more direct linkage than may be immediately apparent. For example, the coral *Lophelia pertusa,* which is the driving organism behind lithoherm formation, precipitates its $CaCO_3$ skeleton from thermocline waters. Recent research has confirmed the plausibility of using *Lophelia pertusa* to create geochemical time series based on stable strontium isotopes (Ruggeberg et al. 2008). This example illustrates the interdisciplinary nature of oceanography, and how a geophysically derived understanding of lithoherm distribution and formation could be used in conjunction with geochemical analysis paleo-water mass properties. In the same regard, this dissertation demonstrates the use of very different methods and approaches in the pursuit of conclusions based within the interdisciplinary frame of oceanography.

CHAPTER II

AAIW $\delta^{13}C$ VARIABILITY DURING THE YOUNGER DRYAS

INTRODUCTION

The expression of the Younger Dryas in the North Atlantic is well documented. Multiple lines of evidence suggest that meridional overturning circulation decreased substantially most likely as the result of meltwater discharge into the zone of NADW formation (Boyle and Keigwin 1987; Broecker 2006; Fairbanks 1989; Keigwin et al. 1991; Marchitto et al. 1998; McManus et al. 2004). However, limited data exist in regard to the expression of the Younger Dryas in the South Atlantic Ocean (Came et al. 2003; Charles and Fairbanks 1992; Pahnke et al. 2008). Seawater PO_4 data implied from the Ca/Cd ratios found in benthic foraminifera from the western subtropical South Atlantic suggest a reduction in deep and intermediate water export from the North Atlantic to the South Atlantic, reconfirming a reduction in northward meridonal heat transport (Came et al. 2003). Neodymium isotope ratios (Fe-Mn oxides) from depths corresponding to the transition between Antarctic Intermediate Water (AAIW)/upper North Atlantic Deep Water (NADW) along the Brazilian Margin and Tobago Basin also reveal a positive excursion coincidental with the Younger Dryas (Pahnke et al. 2008). Though these data indicate a shift in the prevalence of northern source and southern source intermediate waters (and arguably the production rate of AAIW), they do not address how the intrinsic properties of AAIW may have changed in response to the Younger Dryas. Specifically, how did the $\delta^{13}C$ composition of AAIW vary?

Comprehension of the carbon isotopic variability of AAIW is key for several reasons: Most importantly, the $\delta^{13}C$ composition of AAIW records variations in the thermodynamic equilibrium between the water mass and the atmosphere at the time of formation (Broecker and Maier-Reimer 1992; Charles et al. 1993). This equilibrium is influenced by temperature, residence time at the surface, and frictional coupling between the ocean and atmosphere (wind). Combined, these elements are a major factor in controlling the contribution of AAIW to thermocline ventilation and carbon sequestration (Broecker and Peng 1982). In addition, AAIW acts as a key mechanism in transferring $\delta^{13}C$ variability to low(er) latitudes (Ninnemann and Charles 1997).

Here we present $\delta^{13}C$ and $\delta^{18}O$ evidence from a transect of cores taken along the Angolan slope that span the contemporary transition between AAIW and Labrador Sea Water (LSW). The shallowest of these cores has remained within the core of AAIW since before the onset of the Younger Dryas. $\delta^{13}C$ and $\delta^{18}O$ data were derived from the benthic foraminifera *Cibicidoides pachyderma* and age control was established via ^{14}C analysis of mixed planktonic species *Globigerinoides ruber* and *Globigerinoides sacculifer.* These data shed new light on localized water mass geometry, and the intrinsic $\delta^{13}C$ variability of AAIW during the Younger Dryas.

STUDY AREA

Piston core TAMU-005 was taken from the Angolan margin at 11° 55.0113' S, 13° 17.1661' E in 798 m of water. This depth represents the core of AAIW in relation to the contemporary water mass geometry in the Southeast Atlantic (Ostlund et al. 1987;

Schlitzer 2004) (Fig. 1). During the Younger Dryas, this position along the Angolan margin was approximately 65 m shallower based on eustatic sea level (Fairbanks 1989), leaving these sediments still within the core of AAIW (Pahnke et al. 2008). Piston cores TAMU-004, TAMU-003, TAMU-002 and TAMU-001 were taken along a single transect progressing downslope from TAMU-005 at approximately 200 m depth intervals (Table 1). Collectively, the transect spans the contemporary transition zone between AAIW and LSW (Fig. 1).

METHODS

Preliminary $\delta^{18}O$ and $\delta^{13}C$ stable isotope stratigraphies for TAMU-005 – TAMU-001 were determined by processing samples taken at 10 cm intervals spanning the entire length of the core. Sediments were wet sieved at 63 μm to remove the fine grain sediment fraction. The coarse >63 μm sediment fraction was then dehydrated with methanol and oven dried. The planktonic foram *G. ruber* was isolated from the size fraction 212<250 μm (dry sieve). Specimens were then sonicated (at around 38% max power using a rheostat to minimize fracture and disintegration) for approximately ten to twenty seconds until all adhering material was removed. The sonicating liquid (methanol) was then removed from the vial using a syringe and hypodermic needle in order to clear the particulate contaminants from the vial. The specimens were again oven dried. In some cases, small amounts of pyrite and/or clay remained within the test. However, these materials do not pose a threat of contamination with respect to $\delta^{18}O$ and $\delta^{13}C$ analysis. Between three and seven individual forams were analyzed from each

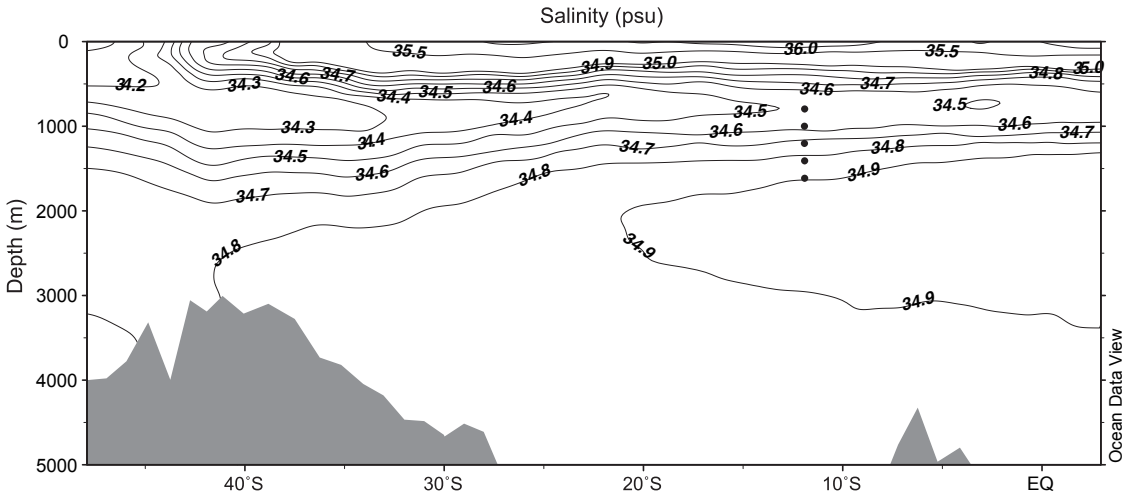

Fig 1.—Location of TAMU core transect (black circles) in relation to modern water mass geometry.

Table 1.— *Core location and recovery.*

Core	Water Depth (m)	Latitude	Longitude	Recovery (cm)
TAMU-005	798	11° 55.0113'S	13° 17.1661'E	290.5
TAMU-004	996	11° 55.0249'S	13° 12.0068'E	399.5
TAMU-003	1199	11° 54.9960'S	13° 06.2697'E	335.0
TAMU-002	1421	11° 55.0081'S	13° 01.1748'E	401.5
TAMU-001	1585	11° 54.9970'S	12° 50.0982'E	421.5

sample using a Finnegan MAT-253/GV Isoprime isotope ratio mass spectrometer (IRMS) equipped with a dual inlet and a Kiel/Gilson style automated sampling device.

Utilizing the chronology obtained from the preliminary stratigraphy, sediment samples were taken at a frequency of every other centimeter for TAMU-005 – TAMU-001 spanning the last glacial maximum (LGM). Sediment samples were prepped in the same manner as described above. The benthic forams *C. pachyderma*, *Planulina ariminensis* and *P. wuellerstorfi* were isolated (>250 μm) for all intervals depending on occurrence within the core. In all cases, *C. pachyderma* was the primary species used for analysis due to the continuity of its occurrence. Single *C. pachyderma* tests were analyzed from each sample for $\delta^{18}O$ and $\delta^{13}C$ using a Micromass Optima IRMS equipped with a dual inlet and a common acid bath style automated sampling device.

In addition to stable isotope chronologies, multiple ^{14}C measurements were obtained for TAMU-005, and single core bottom measurements were obtained for cores TAMU-004, TAMU-003, and TAMU-001 (Table 2). Combined *G. ruber* and *G. sacculifer* tests were used for all analyses. Initial core bottom samples were analyzed at the Lawrence Livermoore Labs accelerator mass spectrometer (AMS) facility. The forams were prepped in the same manner as described above for stable isotopic analysis. Following the acquisition of benthic isotope stratigraphies, two more samples from TAMU-005 were analyzed at the NOSAMS facility at Wood Hole Oceanographic Institution (prepped at Texas A&M per NOSAMS specifications). These samples correspond to the onset and the termination of the $\delta^{18}O$ and $\delta^{13}C$ excursions as determined to be concurrent with the Younger Dryas. All radiocarbon dates were converted to calendar

Table 2.— *Radiocarbon results for TAMU cores including all probabilities based on the radiocalibratioin curve (Stuiver and Reimer 1986-2009).*

Core	Depth (cmbsf)	Species	1-Sigma Range	Probability Factor	Median Age (calendar years)	Weighted Age (calendar years)
TAMU-005	120.5	*G. ruber, G. sacculifer*	11440 - 11465	0.034	11453	11827
			11630 - 12050	0.966	11840	
TAMU-005	128.5	*G. ruber, G. sacculifer*	10764 - 11107	1	10936	10936
TAMU-005	290.5	*G. ruber, G. sacculifer*	18725 - 18831	1	18778	18778
TAMU-004	399.5	*G. ruber, G. sacculifer*	30721 - 30034	1	30378	30378
TAMU-003	335.0	*G. ruber, G. sacculifer*	≥50000	n/a	n/a	n/a
TAMU-001	402.5	*G. ruber, G. sacculifer*	47777 - 45588	1	46683	46683

ages using the Calib Rev 5.0.1 program (Stuiver and Reimer 1986-2005) and the associated Marine Reservoir Correction Database (Stuiver and Reimer 2009).

RESULTS

The high resolution sampling strategy employed for TAMU-005 results in an approximate temporal resolution of 121 years. This is an estimate is based on a whole core average sedimentation rate of 16.6 cm/ka determined from linear interpolation between absolute age control points. This, along with the use of single foram tests results in single point spikes in both the $\delta^{13}C$ and $\delta^{18}O$ records. In spite of the apparent "noise" in this record, this variation is indicative of minimal time averaging, which provides the luxury of determining which events in the record are significant based on two or more constraining points. A lower sampling resolution and use of multiple foram tests would lead to uncertainties about the validity of relatively short duration events in the record.

The most prominent feature in the $\delta^{13}C$ record is the positive excursion between 128.5 and 120.5 centimeters below sea floor (cmbsf), which is defined by three successive data points (Fig. 2). The magnitude of this excursion is 0.59 $^{0}/_{00}$, representing a change roughly equivalent to 58% of the total range in $\delta^{13}C$ between the LGM and Holocene. A positive $\delta^{18}O$ excursion of 0.37 $^{0}/_{00}$ occurs concurrently with the event seen in the $\delta^{13}C$ record and is defined by two successive data points. Radiocarbon dates were collected at 128.5 and 120.5 cmbsf in order to constrain the timing of this event

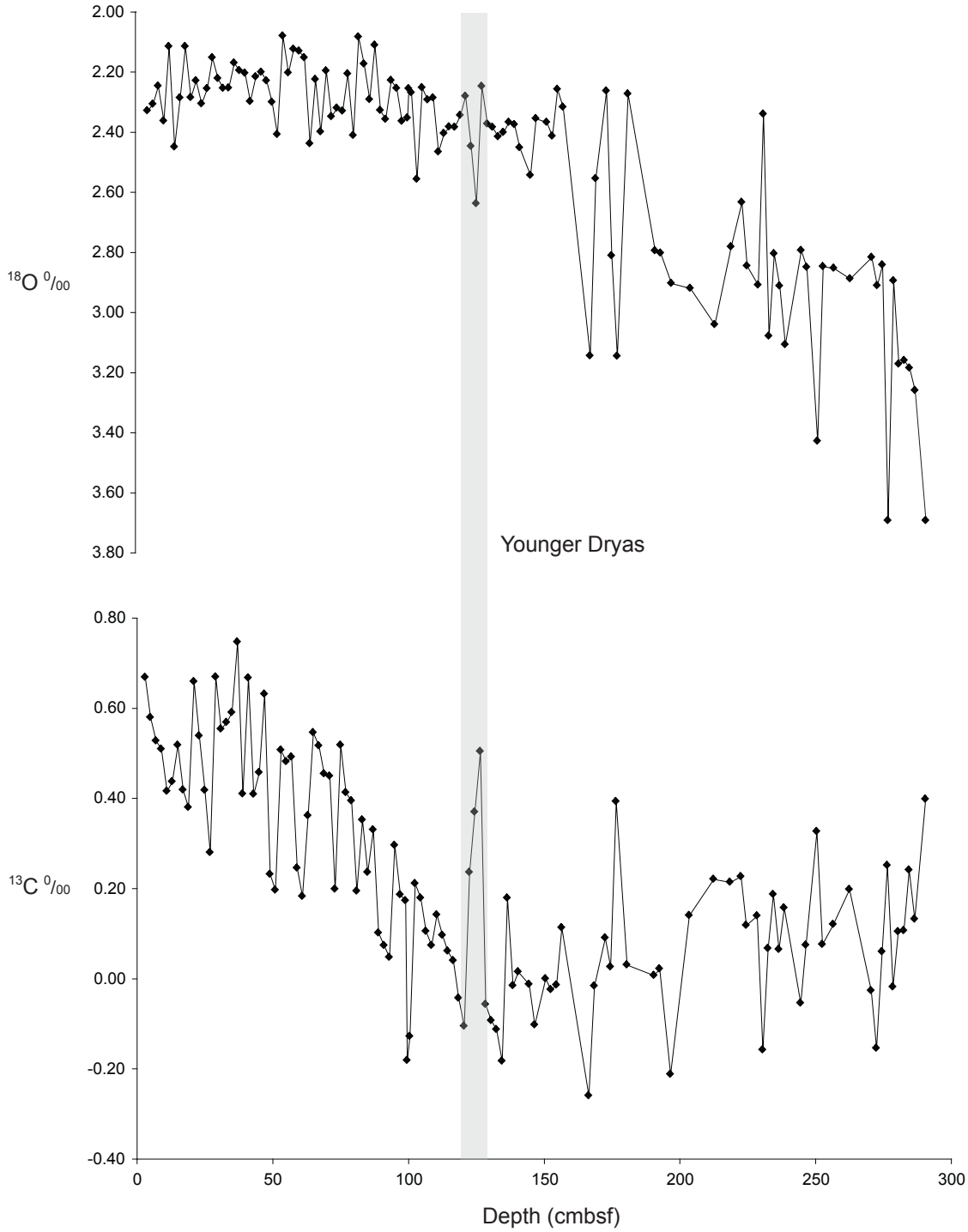

Fig 2.—TAMU-005 benthic foraminiferal isotopic results. Shaded area indicates the position of Younger Dryas.

(Table 2). The timing of the event, based on the average of these two ages, is 11,381 calendar years before present (ybp), which is consistent with the timing of the Younger Dryas (Fairbanks 1989). The age inversion between the 128.5 and 120.5 cmbsf is not unexpected considering the uncertainties in the marine radiocarbon calibration curve during the Younger Dryas (Muscheler et al. 2008). Ocean reorganization, along with an increase in atmospheric radiocarbon, point to the possibility of erroneous reservoir ages. This is especially relevant at the onset of the Younger Dryas (Singarayer et al. 2008). As a result, determining the temporal range of this event is problematic, however, we feel that the approximate timing (as averaged over the duration of the event) is sound.

Though valid core bottom radiocarbon ages were also obtained for TAMU-004 and TAMU-001 (Table 2), the lack of core bottom age control points for TAMU-003 and TAMU-002 (along with variable sedimentation rates) make absolute core-to-core correlation difficult. In lieu of absolute age control, we established relative age control for TAMU-004 – TAMU-001 by direct correlation of the planktonic $\delta^{18}O$ stratigraphies of these cores to the planktonic $\delta^{18}O$ stratigraphy of TAMU-005 (Fig. 3). The reason planktonic foraminifera were used for the age correlation is that these forams all precipitate their tests within a common depth range, and are therefore not as subject to the variable temperature affect associated with depth. The planktonic $\delta^{18}O$ correlation values derived from TAMU-005 are 0.313 $^{0}/_{00}$ (at 290.5 cmbsf) for the 18.8 ka age control point, and -0.859 $^{0}/_{00}$ (at 124.5 cmbsf) for the 11.4 ka age control point. In all but two instances, there was only one possible depth corresponding to the respective correlation values within the other cores (Fig. 3). In the two instances where more than

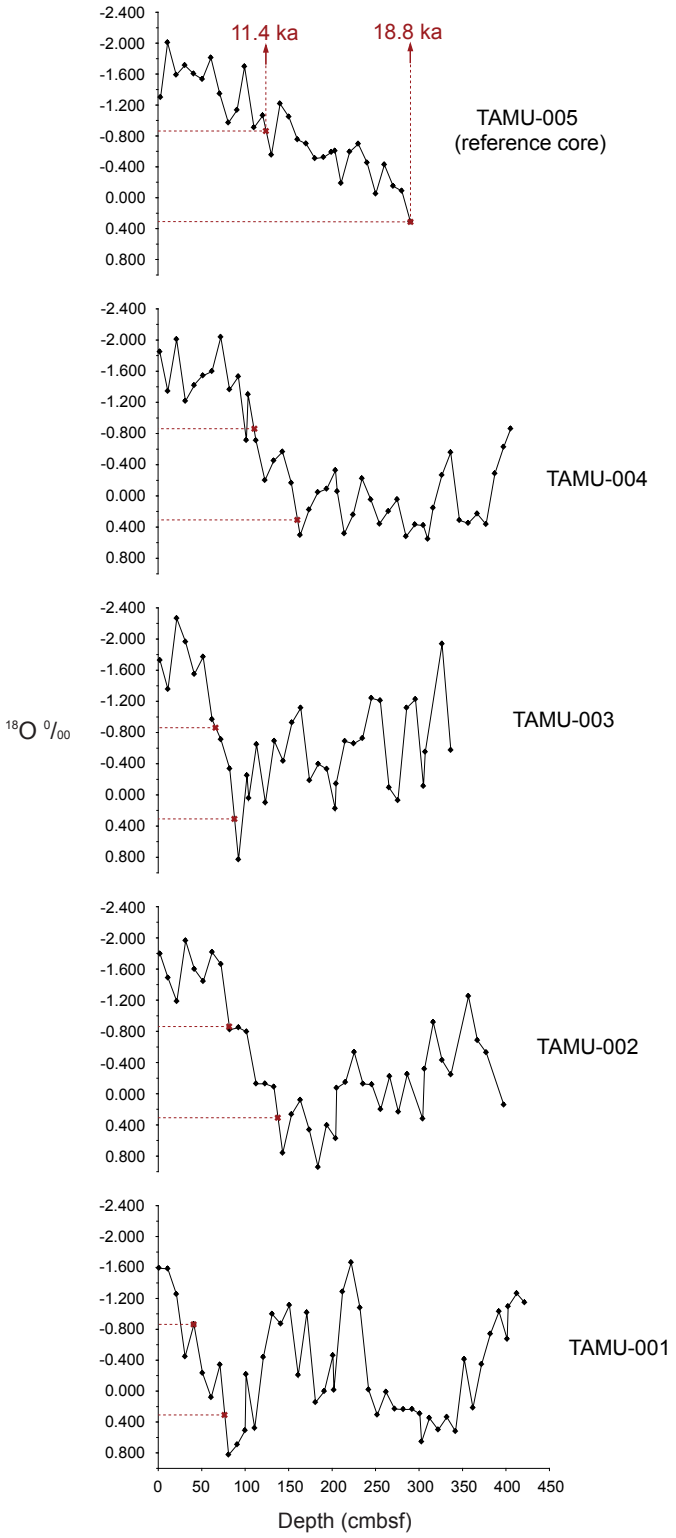

Fig 3.—TAMU-005 through TAMU-001 planktonic foraminiferal $\delta^{18}O$ age correlation. Correlation points are based on ^{14}C ages established for TAMU-005.

one possible correlation point exists, due to the inherent variability of the isotopic record, the deepest occurrence of the correlation value along a positive sloped, well-defined trend was utilized (as can be associated with the overall deglacial trend) (Fig. 3).

Immediately apparent is the variability in sedimentation rate between the cores, and the lack of a clear positive $\delta^{13}C$ excursion (at approximately 11.4 ka) in any other core than TAMU-005 (Figs. 4 & 5). The only ostensible correlation is the strong dip in $\delta^{13}C$ values in TAMU-003, which has no clear counterpart in the associated $\delta^{18}O$ record. $\delta^{13}C$ and $\delta^{18}O$ versus depth profiles are presented at both age control points (18.8 ka and 11.4 ka) based on interpolation between single isotopic measurements (Fig. 6). A late Holocene profile is also presented which represents an average of the top 15 cm of each core. Three very distinct intermediate water mass geometries representing the LGM (18.8 ka), Younger Dryas (11.4 ka) and late Holocene are revealed.

DISCUSSION

Intermediate Water Mass Geometry

While the lack of an independently determined paleotemperature proxy, such as Mg/Ca, makes it difficult to separate inter-water mass temperature/salinity effects in the $\delta^{18}O$ profiles (Fig. 6b), the $\delta^{13}C$ profiles do provide some interesting insights into the intermediate water mass relative geometry during the Younger Dryas (Fig. 6a). Most striking is the similarity of the LGM and Younger Dryas profiles. Both profiles elucidate the presence of a sub-AAIW nutrient maximum centered at approximately 1200 m, where $\delta^{13}C$ was $-0.20\ ^{0}/_{00}$ lower during the Younger Dryas than the LGM. This

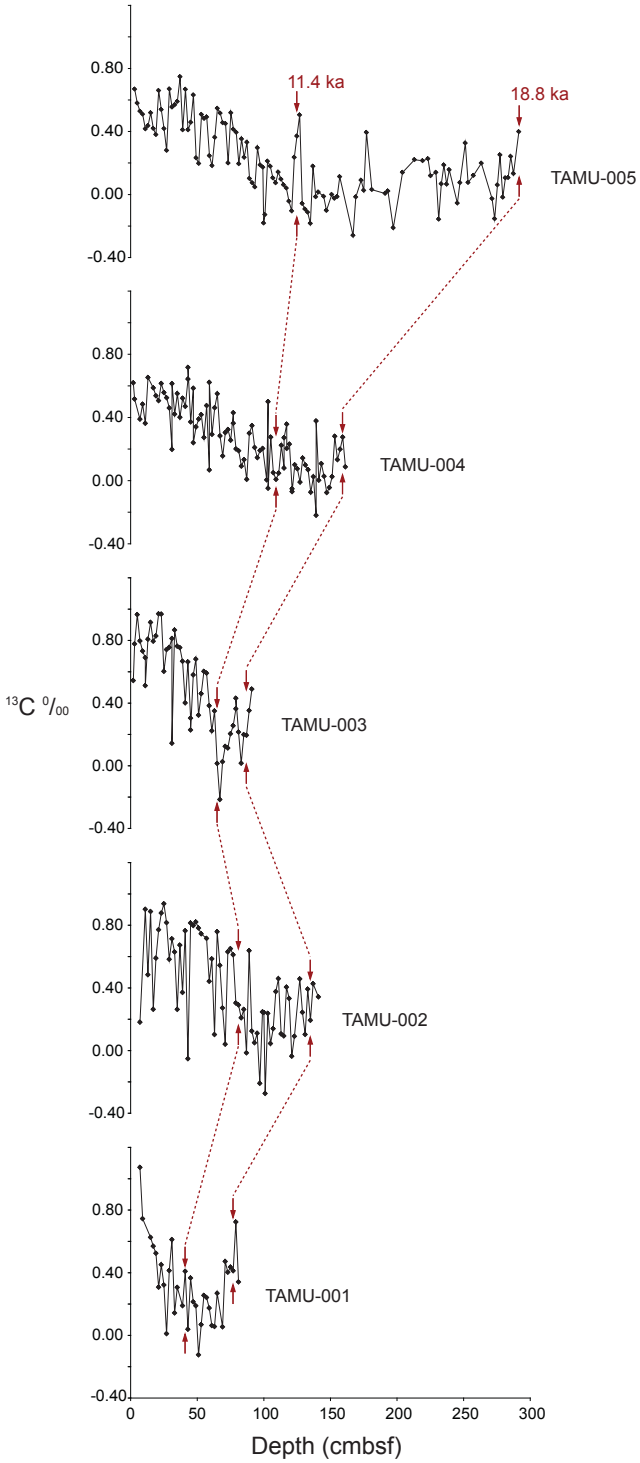

Fig 4.—TAMU-005 through TAMU-001 benthic foraminiferal $\delta^{13}C$ comparison with age control points identified.

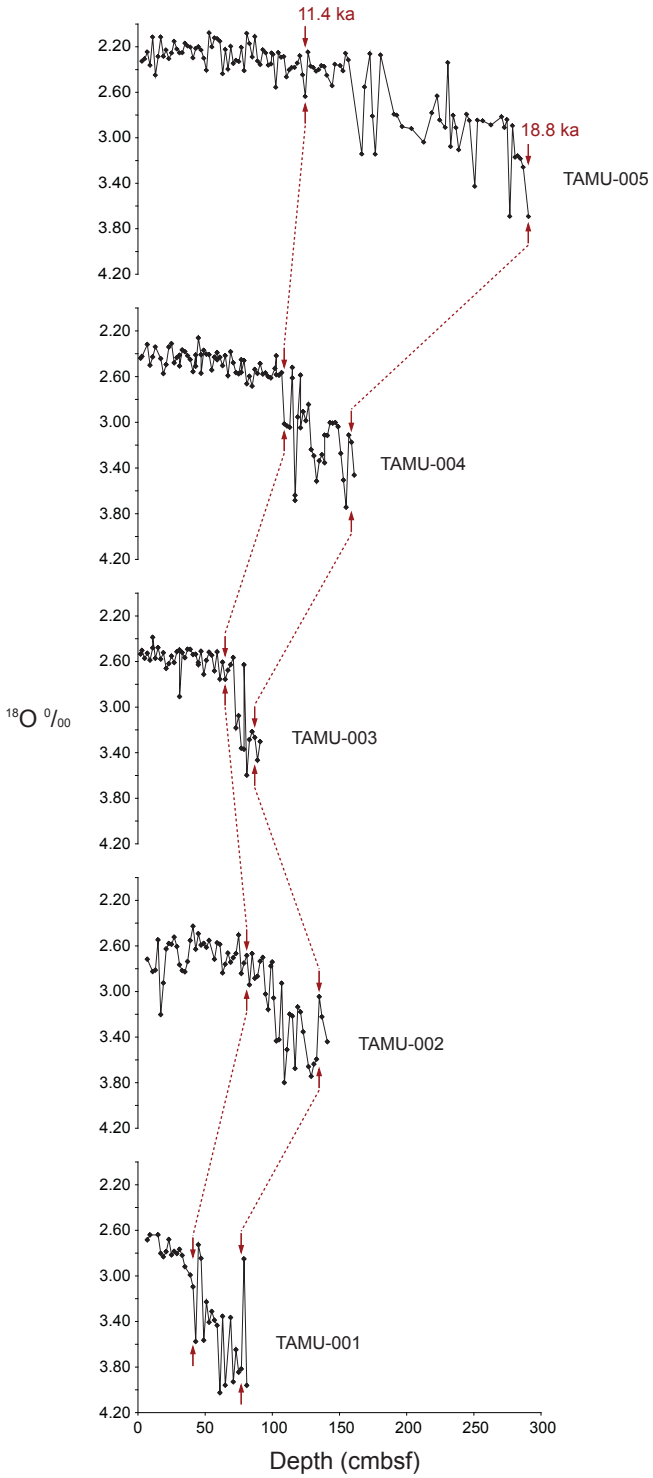

Fig 5.—TAMU-005 through TAMU-001 benthic foraminiferal $\delta^{18}O$ comparison with age control points identified.

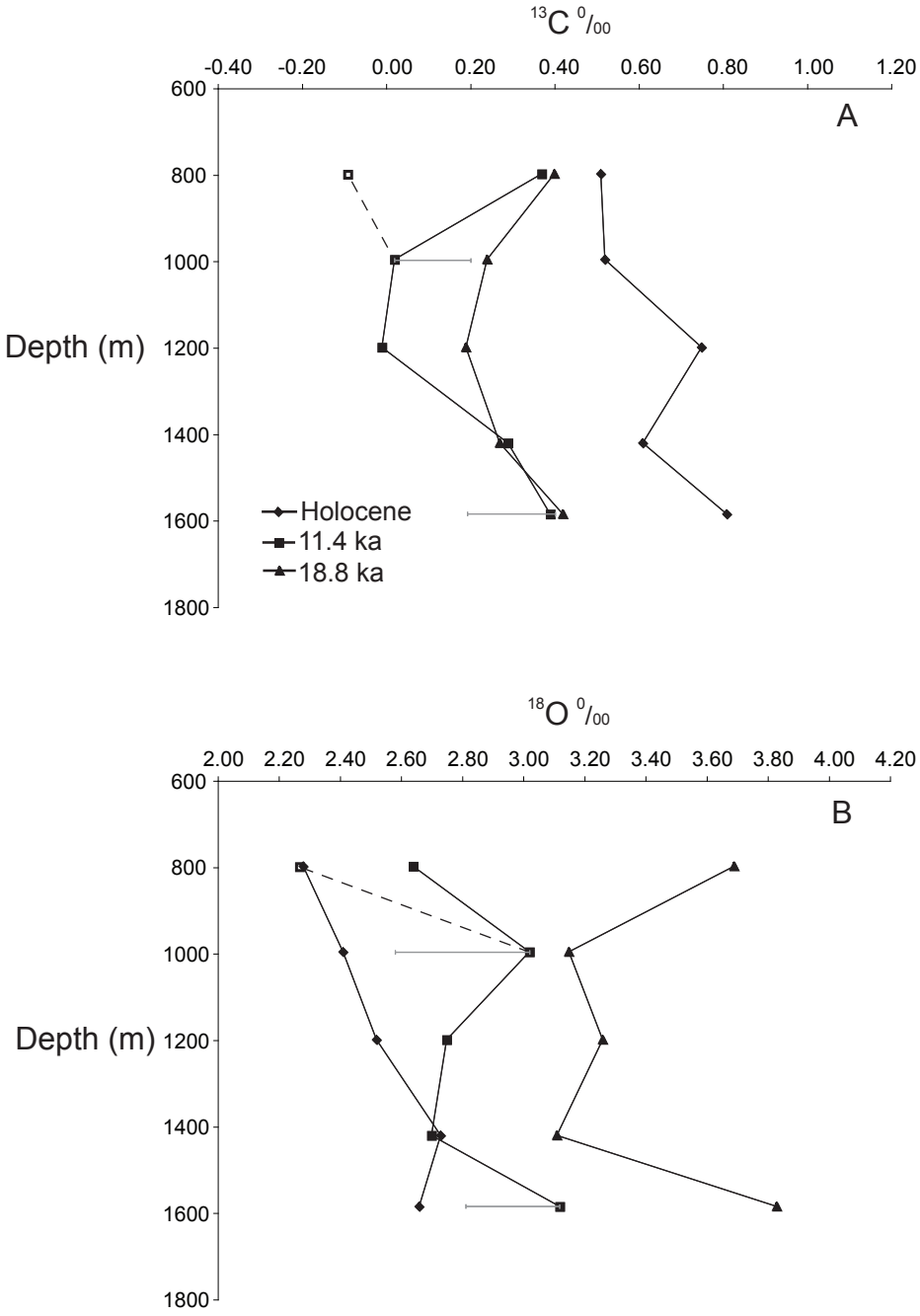

Fig. 6.—$\delta^{13}C$ versus depth (A) and $\delta^{18}O$ versus depth (B) profiles for 18.8 ka (LGM), 11.4 ka (Younger Dryas - median of $\delta^{13}C$ excursion), and the latest Holocene. The open square and dashed line represent the average of the values immediately before and after the 11.4 ka excursion. Grey error bars represent maximum uncertainty due to more than one possible correlation point.

suggests that North Atlantic Intermediate Water (NAIW) export to the south Atlantic may have been more reduced during the Younger Dryas than during the LGM (Boyle and Keigwin 1987; Came et al. 2003; Slowey and Curry 1995). The sharp $\delta^{13}C$ gradient between 800 m and 1200 m at the Younger Dryas implies a well defined vertical segregation of nutrients controlled, at least in part, by inherent variations in the isotopic composition and or production rate of AAIW (Fig. 6a). This is evident when the average $\delta^{13}C$ values of AAIW immediately before and after the Younger Dryas excursion are plotted as a reference point on the $\delta^{13}C$ profile (Fig. 6a).

Possible Mechanisms of AAIW $\delta^{13}C$ Variation

AAIW $\delta^{13}C$, though subject to changes in the overall oceanic carbon reservoir (Curry et al. 1988), is modulated over relatively short time scales by variations in ocean/atmosphere interactions at its point of origin in the Southern Ocean. Here, biological effects and nutrient driven scenarios for $\delta^{13}C$ variability are overprinted by changes in the level of thermodynamic isotopic equilibrium, which is affected by temperature and wind stress (Broecker and Maier-Reimer 1992; Charles et al. 1993; Libes 1992; Ninnemann and Charles 1997). Beyond these factors affecting the "preformed" $\delta^{13}C$ value of AAIW, are those that lead to variability while in transit along the isopycnal surfaces at the base of the thermocline, and the localized factors that influence nutrient concentrations at 11° 55.0113' S, 13° 17.1661' E where TAMU-005 was taken (Fig 7). Below, we consider the mechanisms involved in the 0.59 $^{0}/_{00}$ $\delta^{13}C$

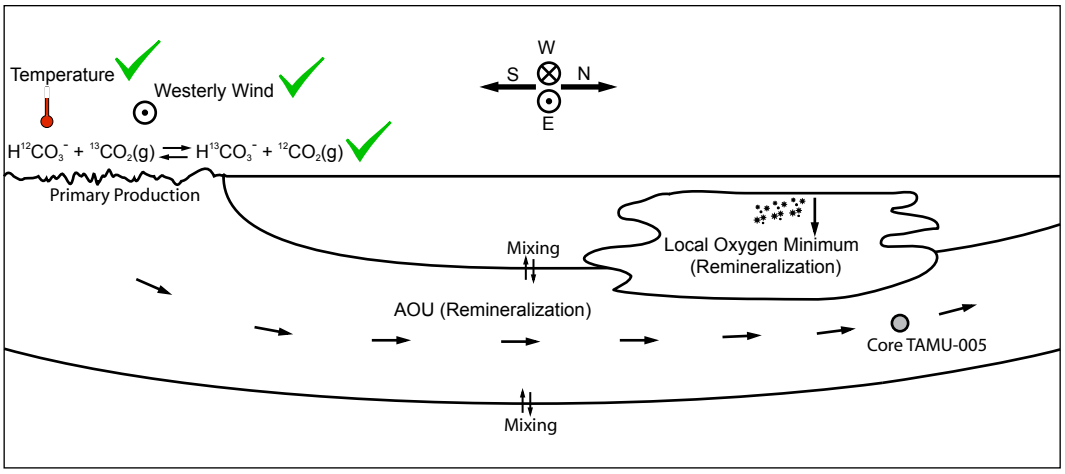

Fig. 7.—Schematic illustrating the factors that influence AAIW isotopic variability. Green check marks identify the dominant contemporary influences.

excursion of AAIW during the Younger Dryas (Fig 2). Beyond the obvious significance of the timing, we chose to focus on this part of the record because it represents the only event characterized by simultaneous excursions in both the $\delta^{13}C$ and $\delta^{18}O$ records defined well by multiple successive points.

Thermodynamic Effect Due to AAIW Temperature.— The most direct mechanism for AAIW $\delta^{13}C$ variability is evidenced in the associated 0.37 $^{0}/_{00}$ $\delta^{18}O$ excursion. Around 11.4 ka, sea level was approximately 65 m below the current level, and the mean ocean $\delta^{18}O$ was 0.67 ±0.05 $^{0}/_{00}$ greater than today (Fairbanks 1989). Utilizing GEOSECS Site 107 (Ostlund et al. 1987) data, we determined the contemporary $\delta^{18}O$ value (near the TAMU-005 core location), and what it would be if sea level were 65 m shallower than it is today. From this, we formulated the following mass balance:

$$\delta^{18}O_{Wyd} = \delta^{18}O_{Wcurrent} + \Delta\,\delta^{18}O_{depth} + \Delta\,\delta^{18}O_{ice}$$

where $\delta^{18}O_{Wyd}$ is the oxygen isotopic value of ocean water at 11.4ka at 733 m depth, $\delta 18O_{Wcurrent}$ is the current oxygen isotopic value at 798 m depth, $\Delta\,\delta^{18}O_{depth}$ is the change due to sea level (based on current values), and $\Delta\,\delta^{18}O_{ice}$ is the change due to ice volume. When values are substituted in:

$$\delta^{18}O_{Wyd} = (-0.18) + (0.01) + (0.67) = 0.50 \pm 0.05\ ^{0}/_{00}.$$

Using *C. pachyderma* core top $\delta^{18}O$ values from TAMU-005 – TAMU-001 (average of top 15 cm), we assessed multiple paleotemperature equations in order to find the best fit for our data. The most accurate equation was that of Bemis et al. (Bemis et al. 1998), which we used to compare temperature values calculated from our core tops to those recorded at GEOSECS Site 107(Ostlund et al. 1987). Linear regression yields an R^2 value of 0.84, which is slightly lower than it should be due to a small error between Sigma T GEOSECS values and calculated values for temperature (≤ 0.15 °C between 800 m and 1600 m) (Fig. 8).

Applying the paleotemperature equation to the 0.37 $^{0}/_{00}$ $\delta^{18}O$ excursion yields a change in temperature of -1.8 ±0.24 °C. If this change in temperature were imparted at the zone of AAIW formation, the equivalent thermodynamic fractionation effect would be a 0.22$^{0}/_{00}$ $\delta^{13}C$ enrichment of aqueous bicarbonate (HCO_3^-) relative gaseous carbon dioxide (CO_2) (Mook et al. 1974), hence enriching AAIW at the point of origin.

AOU, the Oxygen Minimum, and Localized Changes in Productivity.— Based on the regression equation of Kroopnick (Kroopnick 1985), and contemporary calculations of apparent oxygen utilization (AOU) (Schlitzer 2004), the effect of organic carbon remineralization while AAIW travels from around the Antarctic polar front (APF) to the low latitude South Atlantic is completely overprinted by thermodynamic effects. The contemporary value for $\delta^{13}C$ at the core location is 0.56 $^{0}/_{00}$ (Ostlund et al. 1987), corresponding closely to the phosphate normalized value of 0.54 $^{0}/_{00}$ (Charles et al. 1993). However, the expected $\delta^{13}C$ value based on AOU is -0.04 $^{0}/_{00}$. This large

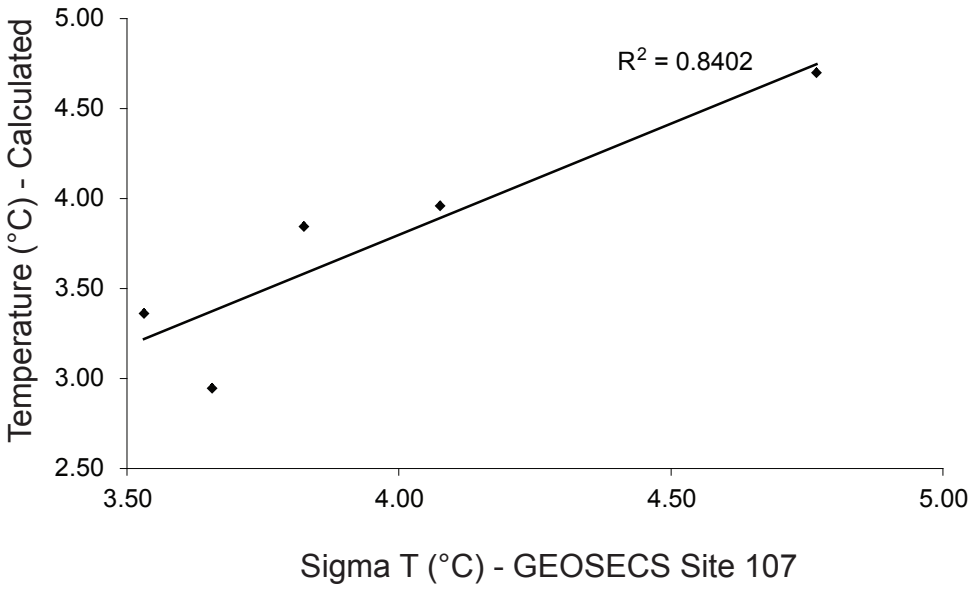

Fig 8.—Core top calibration based on calculated temperature from TAMU-005 - TAMU-001 (Bemis et al. 1998) and actual data from GEOSECS Site 107. For GEOSECS Site 107, T - Sigma T ≤ 0.15 °C from 800m - 1600m.

discrepancy confirms the dominant influence of air sea exchange over the $\delta^{13}C$ signature of AAIW. Therefore, we consider the effect of organic carbon remineralization incurred along the path of AAIW between the APF and low latitude South Atlantic to be constant over the time scales associated with this circulation.

Localized effects of organic carbon remineralization into the water column must also be considered due to the occurrence of TAMU-005 within the Benguela upwelling region, and the associated oxygen minimum. The two major factors that could affect the $\delta^{13}C$ signature at the TAMU-005 location are the depression of the oxygen minimum due to the lowered sea level (lowering of $\delta^{13}C$) and a large decrease in export production. A depression of sea level at the Younger Dryas of 65 m would lead to a -0.03 $\delta^{13}C$ change based on contemporary water column values (Ostlund et al. 1987; Romanek et al. 1992). Even in this scenario, TAMU-005 would still be below the core of the oxygen minimum zone. Sediment records from the region indicate that during the Younger Dryas, export production actually increased due to an increase in equatorial trade wind strength (Farmer et al. 2005). Therefore, even though we cannot conclude an absolute change in the extent of the oxygen minimum, we can conclude a reduction in organic carbon remineralization would not have occurred and led to a localized increase in $\delta^{13}C$. We can also conclude that changes in the relative depth of TAMU- 005 due to sea level fluctuations (between the Younger Dryas and late Holocene) would not have significantly affected $\delta^{13}C$ variability.

Additional Mechanisms of $\delta^{13}C$ Variability?— If we consider all of the above factors in regard to the observed Younger Dryas $\delta^{13}C$ excursion of 0.59 $^{0}/_{00}$, the only significant, or at least quantifiable, influence is that of a temperature reduction at the point of origin as determined from the associated $\delta^{18}O$ excursion. As a 1.8 °C drop in temperature accounts for only 0.22 $^{0}/_{00}$ Δ $\delta^{13}C$, we are left with 0.37 $^{0}/_{00}$ to explain. To this end, Broecker and Maier-Reimer (Broecker and Maier-Reimer 1992) carried out a Hamburg ocean general circulation model in order to determine the sensitivity of air-sea exchange rate on the $\delta^{13}C$ thermodynamic enrichment throughout the world's oceans. This was accomplished by doubling the wind velocities over the entire ocean. In theory, this doubling increases the efficiency of the thermodynamic fractionation exchange equilibrium by increasing surface area at the ocean/atmosphere boundary (waves and turbulence) (Broecker and Peng 1982; Libes 1992). Though the same process causes bubble injection and the bulk input of light CO_2, the temperature driven thermodynamic preference of the heavy carbon isotope in aqueous HCO_3^- (relative to both gaseous and aqueous CO_2) at low temperatures may result in a net positive shift in the bio-available dissolved inorganic carbon (DIC) reservoir. As expected, the model suggests that in the area of AAIW formation (characterized by cool temperatures and high PO_4), a doubling of the wind induced air-sea exchange rate would result in approximately 0.4-0.8 $^{0}/_{00}$ $\delta^{13}C$ enrichment. Such an increase in the strength of the southern westerlies could explain the remaining 0.37 $^{0}/_{00}$ enrichment noted in TAMU-005. In the same sense, an increase in wind velocity could also account for a reduction in temperature due to greater heat flux from the ocean to atmosphere (Sverdrup et al. 1942), potentially explaining a portion of

the 0.22 $^{0}/_{00}$ $\delta^{13}C$ enrichment currently associated with the 0.37 $^{0}/_{00}$ $\delta^{18}O$ enrichment. And, in fact, new evidence suggests that during the Younger Dryas, Patagonian glaciers advanced not primarily as the result of decreased temperature, but due to increased precipitation on the eastern side of the Andes resultant from a focusing of the Southern Westerlies between 45° S and 50 ° S (Ackert et al. 2008). The focusing of Southern Westerlies between 45° S and 50 ° S would also increase Eckmann pumping at the locus of AAIW formation, increasing the injection rate to the base of the thermocline (Pond and Pickard 1983). Evidence for this affect is found in a neodymium isotopic record from the Tobago Basin that shows an approximate 1.25 increase in ε_{nd} values during the Younger Dryas (Pahnke et al. 2008). The enrichment in AAIW $\delta^{13}C$, along with increased injection to the thermocline should be considered as a significant source of the observed variability of low latitude nutrient concentration, and hence SST estimations at low latitudes during the Younger Dryas (Ninnemann and Charles 1997; Wan et al. 2008).

CONCLUSIONS

Our results indicate the presence of a strong vertical gradient in $\delta^{13}C$ during the Younger Dryas cooling event. The data suggest that NAIW export to the south Atlantic may have been more reduced during the Younger Dryas than during the LGM. However, inherent $\delta^{13}C$ variability and or increased production of AAIW likely exerted dominant control of the sharp nutrient gradient. A portion of the $\delta^{13}C$ variability (0.22 $^{0}/_{00}$) can be explained by a shift in thermodynamic equilibrium concurrent with a drop in

temperature of 1.8°C at the locus of Antarctic Intermediate Water (AAIW) formation (as derived from the associated $\delta^{18}O$ increase) (Mook et al. 1974). The remaining 0.37 $^{0}/_{00}$ increase in $\delta^{13}C$ most likely resulted from increased wind velocities, and a greater coupling between the ocean and the atmosphere at the locus of AAIW formation (increased efficiency of the thermodynamic process) (Ackert et al. 2008; Broecker and Maier-Reimer 1992). This wind induced variability, and subsequent increase in Eckmann induced injection of AAIW to the base of the thermocline, may help explain observed nutrient variability at low latitudes during the Younger Dryas (Ninnemann and Charles 1997; Wan et al. 2008).

CHAPTER III

A QUANTITATIVE ASSESSMENT OF THE DISTRIBUTION AND MORPHOLOGIES OF LITHOHERMS IN THE STRAITS OF FLORIDA

INTRODUCTION

Direct observations of deep-water coral mounds or "lithoherms" on the seafloor of the Straits of Florida were first made from the submersible *DSRV Alvin* by Neumann et al. (1977). Their observations revealed that features imaged as hyperbolic reflections by seismic systems on ships and, until then, thought to be slump blocks or other erosional features produced by mass wasting of the margin of the Bahamas were actually mounds of carbonate sediments covered by a community of corals and other deep-water organisms. These features represent an important type of modern deep-water coral reef ecosystem (Reed 2002; Reed et al. 2006). Deep-water reef habitat is under increased stress by fishing and other human activities (Fosså et al. 2002; Reed et al. 2007; Roark et al. 2009). A necessary step to recognizing, protecting and managing this biological resource is to determine the distribution of the coral mounds and the environmental factors that influence them (Miller et al. 2009; Munoz et al. 2009). Modern deep-water coral mounds may also provide a valuable analogue or point of contrast for understanding carbonate mound structures found in the geologic record. For example, "mud mounds" found in Lower Cretaceous and Mississippian formations located in northeastern Mexico and south central New Mexico (Dorobek and Bachtel 2001; Murillo-Muneton and Dorobek 2003) and "biogenic mounds" found in seismic records

from the Great Australian Bight (Feary and James 1998) may represent very similar deep-water coral formations. Investigators have, therefore, tried to better understand the features of deep-water coral mounds and their relation to the physical environment at the seafloor. Observations and analyses of samples obtained by submersible and rock dredge provide valuable information about biologic and lithologic aspects of the lithoherms; however, because of limitations of these methods, much less is known about the morphology of lithoherms. Investigators have recently begun using high-resolution marine geophysical approaches to investigate deep-water coral mound structures in the Straits of Florida (Grasmueck et al. 2006).

Modern deep-water coral mounds are not restricted to the Straits of Florida; they occur in other areas of the North Atlantic and similar features exist throughout the world's oceans (Armstrong and van den Hove 2008; Bjerager et al. 2010; Breeze and Fenton 2007; Cordes et al. 2008; Dorschel et al. 2007; Eisele et al. 2008; Fosså et al. 2002; Heifetz 2002; Hovland et al. 2002; Messing et al. 2008; Munoz et al. 2009; Schroeder 2002; Titschack and Freiwald 2005). For example, observations have been made of modern cold water coral mounds and buried relict carbonate mounds along the southwest and northeast Rockall Trough margins in the northeast Atlantic Ocean (Kenyon et al. 2003; van Weering et al. 2003). Measured current velocities, mound orientations, faunal distributions, and sediment accumulations of the Rockall Trough mounds reveal the scenario for their formation and maintenance is similar to that of the Straits of Florida lithoherms (de Haas et al. 2009; Dolan et al. 2008; Mienis et al. 2007; Mienis et al. 2006; Wheeler et al. 2008). Specifically, mound growth and morphology

have been described as a function of increased current velocity and bedload transport. The proposed genesis of these mounds, whether via fluid expulsion features or pre-existing bathymetric highs, (Mienis et al. 2006; Wheeler et al. 2008) remains uncertain. And (most relevantly), morphologic variability, though characterized in regard to length to width ratio, is relatively unconstrained (Wheeler et al. 2008).

The idealized lithoherm envisioned by Neumann et al. (1977) is a deep-water coral mound elongated parallel to the direction that seawater flows along the seafloor (Fig. 9). A crust of partially lithified cemented sediments may encase portions of the mound, particularly the end of the mound that faces the current, providing a hard substrate that is colonized by filter-feeding benthic organisms that act as baffles, trapping suspended sediments so the feature grows over time into the current. Aspects of this model have been tested during investigations conducted using the submersibles *Alvin* and *Johnson Sea-Link*, which allow detailed observation and sampling of specific portions of individual lithoherms. Results of such efforts show that the communities of organisms on lithoherms are zoned in a consistent fashion, with predominately *Lophelia* ahermatypic corals at the up-current end, *Zoanthid* sea fans at the apex, and crinoids and *Alcyonarian* sea pen corals elsewhere (Messing et al. 1990). A number of studies have documented the details of the reef habitat and fauna (Reed 2002; Reed et al. 2006). Petrographic evidence indicates the processes of seafloor cement precipitation and its widespread occurrence (Wilber and Neumann 1993). Cement crusts are dominantly high magnesium calcite, whereas the unconsolidated sediments accumulating over the crust are largely aragonite (Paull et al. 2000; Wilber and Neumann 1993). The

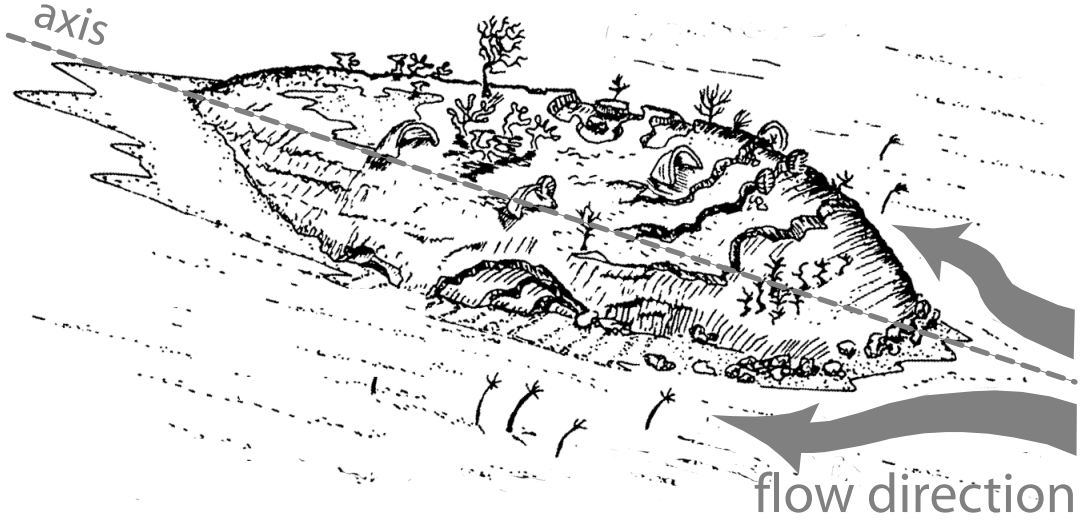

Fig. 9.—The idealized lithoherm is mound of the skeletal remains of organisms and other sediments bound (at least in part) by carbonate cementation that is elongated parallel to the direction of seafloor currents (modified from Neumann et al. 1977).

differences between the ^{14}C ages of these sediments and adjacent living corals are consistent with lithoherm growth due to the trapping of sediments by the organisms (Paull et al. 2000). Much has been learned about the lithoherms in this fashion; however, it has been difficult to investigate aspects of their morphology because submersible observations are inherently limited in their spatial extent and it is difficult for submersibles to maneuver when subjected to the strong currents of the Florida Straits.

Echosounders and other seismic reflection techniques employed from ships at the sea surface show that lithoherms along the southeastern margin of North America typically occur at water depths of 600 m to 800 m and their maximum height ranges typically from 30 m to 50m (as great as 150m relief reported) (Neumann et al. 1977; Paull et al. 2000; Reed et al. 2006). However, in these water depths, the spatial resolution of data obtained by these techniques is insufficient to image lithoherms in the detail necessary to characterize their morphologic features. In 1993, Paull and co-workers acquired among the first images of whole lithoherms when they used the submersible *NR-1* to deploy an analog, side-scan sonar near the seafloor of the Florida-Hatteras Slope. They used this analog data in combination with echosounder bathymetry to estimate not only the height, but the length and orientation of lithoherms (Paull et al. 2000).

Recently available computer-integrated, digital sonar systems make it possible to image and investigate the morphology of seafloor features to a far greater extent than was possible before. This paper presents an analysis of sonar data acquired when the *NR-1* conducted a survey of deep-water coral mounds in the northeastern Straits of

Florida. Aspects of the morphology of over 200 individual mounds and their distribution on the seafloor are quantitatively characterized. At this site, a consistent relationship exists between coral mound morphology and current velocity.

METHODS

We surveyed an approximately 10.92 km^2 area of the seafloor in approximately 650 m of water west of Little Bahama Bank (Fig. 10). This region was selected because it is in the vicinity of the 1971 *Alvin* dives discussed by Neumann et al. (1977) and so would be ideal for investigating the actual morphologies of deep-water coral mounds in the Straits of Florida as well as their relationship to bottom water flow. Data were collected using a 150 kHz Sea Scan PC side-scan sonar system (Marine Sonic) that was deployed from the US Navy's *NR-1* submarine. The *NR-1* submarine is nuclear powered and not subject to the spatial and temporal limitations of battery powered submersibles. Specifically, battery powered submersibles only have the stored energy to sustain life support systems for a period of hours, and only a limited spatial range due not only to energy limitations, but limitations of the propulsions system itself. Since the NR-1 is nuclear powered, the submarine was able to stay on location for approximately 18.5 hours, and maintain a survey speed of approximately 1 to 3 knots. Ten parallel lines of data were collected, which were approximately 3.5 km long each with a swath width of 150 m for each channel. The overlap between adjacent lines of data was approximately 20 m.

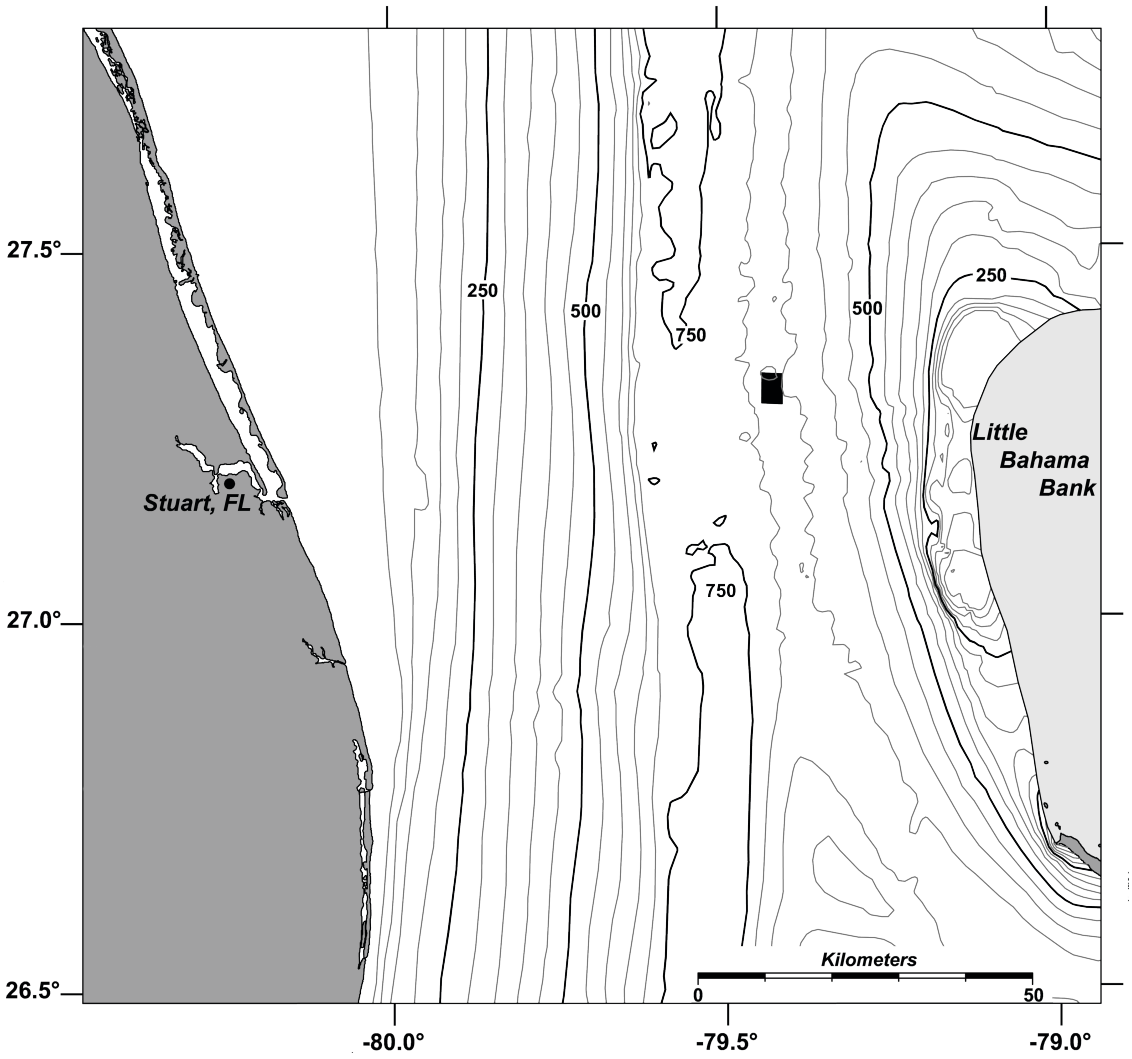

Fig. 10.—General bathymetry map for the Straits of Florida (WGS84,UTM Zone 17N projection-latitude and longitude provided for reference purposes, contours produced from data acquired from the National Geophysical Data Center). The lithoherm survey area is delineated by the black rectangle west of Little Bahama Bank (NW corner: 27.3295º N, 79.4366º W; SE corner: 27.2957º N, 79.4075º W).

In the laboratory, all side-scan files were manually bottom tracked (the altitude of the sonar fish was determined based on first sonic return, or beginning of the sonar image) and slant range corrected using SonarWeb software. The resultant geo-referenced J-peg files were then manually mosaiced in AutoCAD Map 3D to create a mosaic with the best possible transitions (greatest number of features revealed v. covered up) between adjacently overlapping lines (Fig. 11). This mosaic provides a detailed image of the seafloor in the survey area, allowing features to be identified and their overall orientation and spatial relationships to be assessed. For this study, our criteria for identifying a lithoherm was a raised, reflective body composed of one or more elongated structures.

Lithoherms were identified, and then aspects of their morphologies were measured by examining individual lines of data using SeaScan PC review software (native to MST file format). The use of individual lines of data is important because it precludes biases that might otherwise be introduced during the process of mosaicing the data. Because the sonar data are geo-referenced, it was possible to establish the latitude and longitude of both the head and tail ends of each lithoherm, allowing its geographic location to be cataloged and its orientation relative to the seafloor to be determined. The length, height, width, and footprint area of each individual lithoherm were measured from digital sonar data. This approach is based upon established geometric relationships between the sonar, the seafloor, the seafloor feature, and the resultant acoustic travel time and intensity measured by the sonar (Fish and Carr 1990; Johnson and Helferty 1990; Trabant 1984). Because of the relatively high relief of the lithoherms (~6.5 m conservative average) compared to the altitude of the side-scan sonar sensors (target

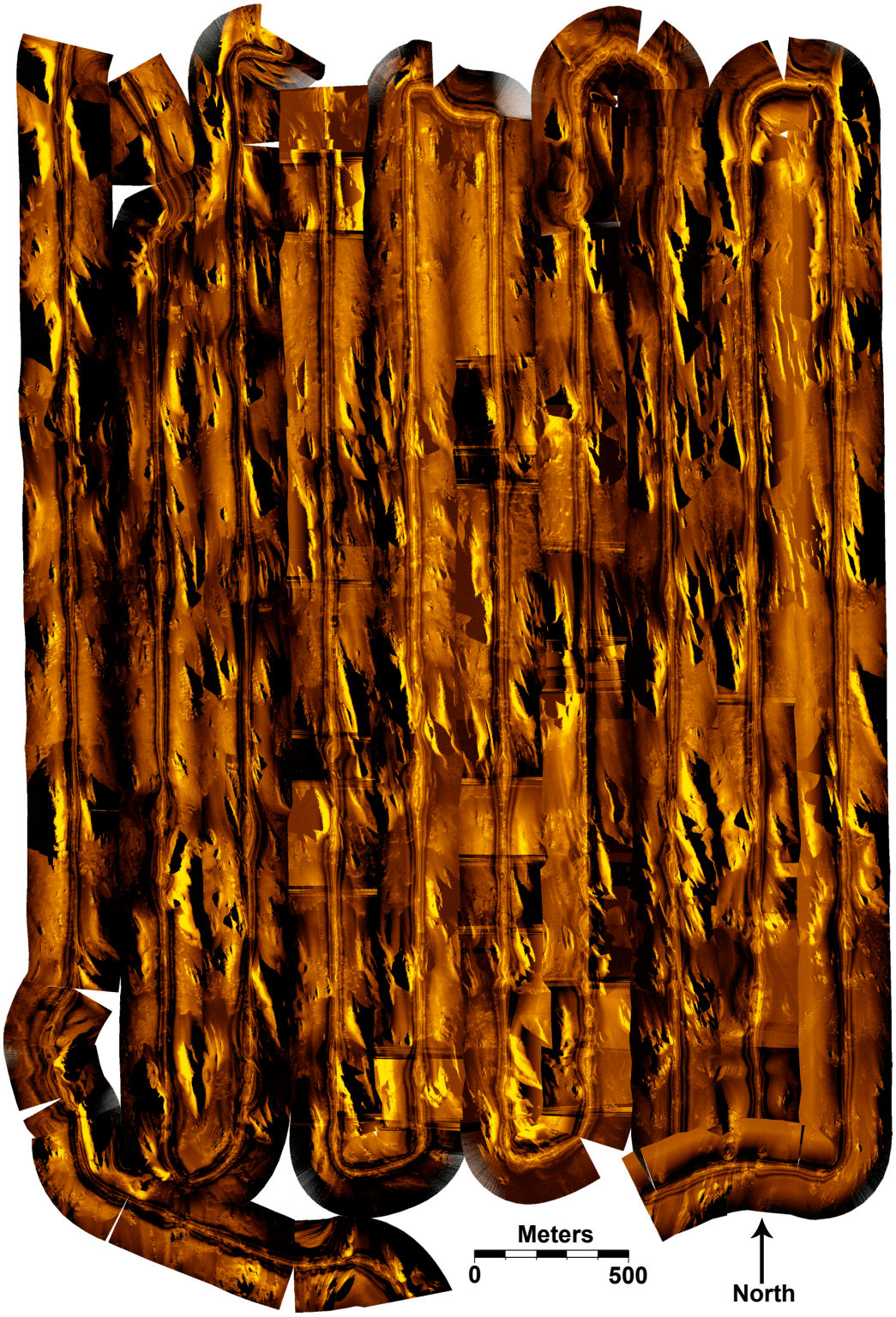

Fig. 11.—Side-scan sonar mosaic of the survey area illustrating lithoherm distribution, orientation and morphology.

altitude = 15 m) the angle of incidence of the sound waves was low, resulting in long across track shadows. And, since the survey lines were run in a north-south orientation, roughly parallel to the lithoherms long axis, the subsequent sound shadows typically obscured the distal slope of each lithoherm. To account for this, individual lithoherms were measured in terms of ½ width and ½ area based on the presumption that these features demonstrate bilateral symmetry. These measurements were multiplied by two to obtain the total width and total area of the lithoherms. Analysis of the morphology of specific features imaged on several survey lines from several orientations demonstrated that this approach was reasonable (Fig. 12).

ANALYSIS AND DISCUSSION

Detailed examination of the side-scan sonar data indicates that 216 individual lithoherms occur within the 10.92 km^2 survey area. Thus, the concentration of lithoherms on the seafloor is approximately 20 lithoherms per square kilometer, which is about 60 times greater than previous estimates of lithoherm concentration on the Florida-Hatteras Slope (1 lithoherm/3 km^2) (Paull et al. 2000). The location of each lithoherm was cataloged, and its general morphologic features were characterized (Table 3) (Fig. 13). These results suggest that the majority of the lithoherms characterized in this study are smaller than those described in previous investigations (Mullins et al. 1981; Neumann et al. 1977; Paull et al. 2000; Reed et al. 2006). For example, the compilation of Reed et al. (2006) indicates that the smaller coral mounds/lithoherms found off the east coast of Florida are approximately 12 m in relief, whereas the majority of

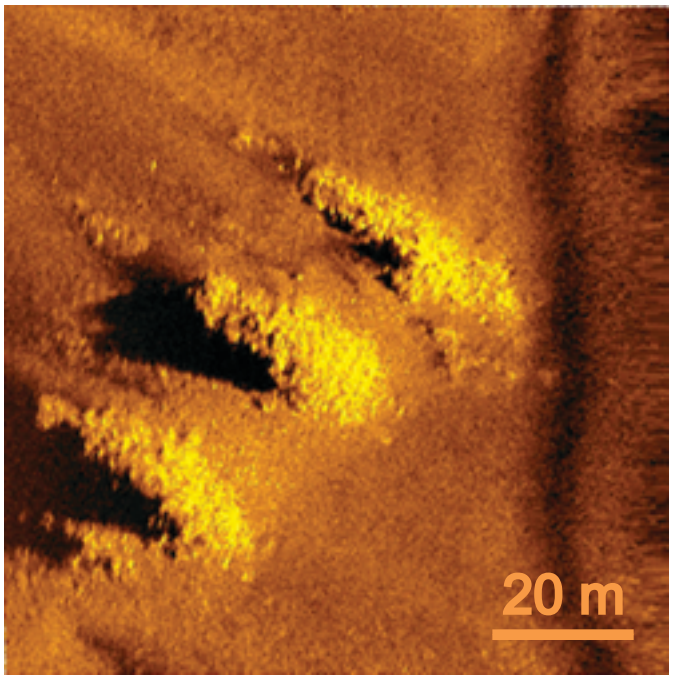

Fig. 12.—Example of lithoherm symmetry obtained as the side-scan sonar swath was at an approximate 45° angle to the lithoherm long axis (obtained as the submarine exited the survey area).

Table 3.— *Descriptive statistics of lithoherms measured in this study.*

Variable	N	Range	Minimum	Maximum	Mean	St. Dev.
Length (m)	210	522.8	28.3	551.1	172.8	112.7
Total Width (m)	211	165.1	8.2	173.3	37.0	28.1
Total Area (m^2)	209	39977.0	220.0	40197.0	6063.2	7587.0
Height (m)[1]	204	16.4	0.8	17.3	6.5	3.2

1) Height represents minimum estimates in some cases.

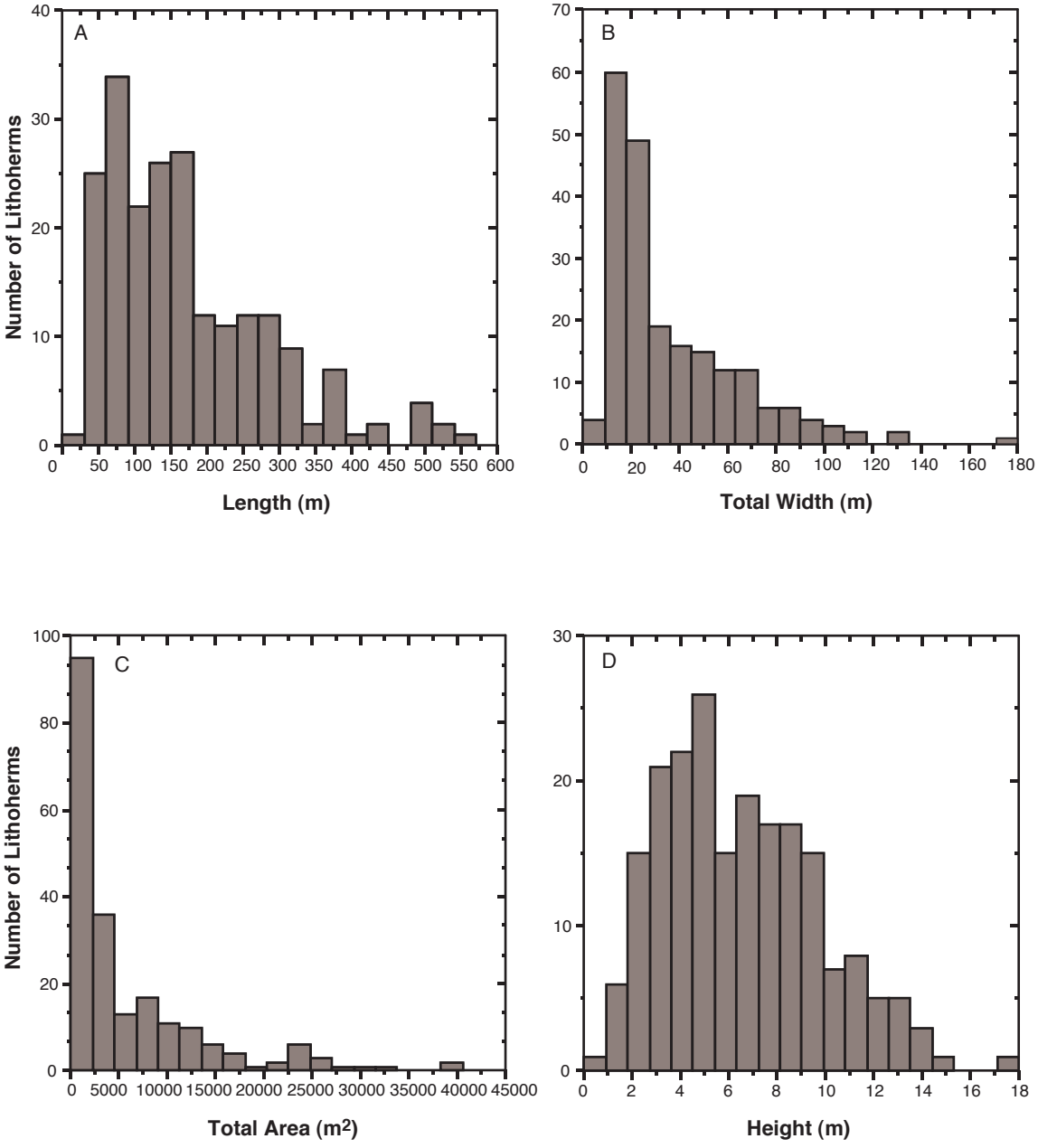

Fig. 13.—Morphology statistics for the measured lithoherms. A) Length; B) total width; C) total area; D) height.

lithoherms described in this study are approximately half (6.5 m) this height. This discrepancy is likely the result of previous data sets being skewed towards the larger lithoherms. It is probable that smaller lithoherms were simply not resolved in significant numbers such as to be included in previous statistics.

Height measurements do represent a limitation of this data set, but on the opposite end of the spectrum than mentioned immediately above. Specifically, height measurements for approximately 24% of the larger lithoherms represent minimum estimates resulting from the sound shadow extending beyond the side-scan swath width. Therefore, it should be noted that heights of the larger features have not been constrained. However, large lithoherms did have heights in excess of 17 m. We know this because sound shadows truncated at the edge of the swath width yield minimum height measurements up to 17 m.

The lithoherms display a range of morphologies. We classified the lithoherms based upon a first order distinction between their morphologies: lithoherms that possess an elongated teardrop shape (singular) (Fig. 14), or a recognizable variation resulting from the accretion of several lithoherms into a larger singular body (fused), which is evident from inspection of the images (a detailed analysis of the accretionary process is in preparation and will be presented elsewhere). A close geometric approximation to the teardrop shape of an idealized lithoherm is a piriform (O'Connor and Robertson 2004). The equation for which is:

$$B^2 \times Y^2 = X^3 \times (A - X)$$

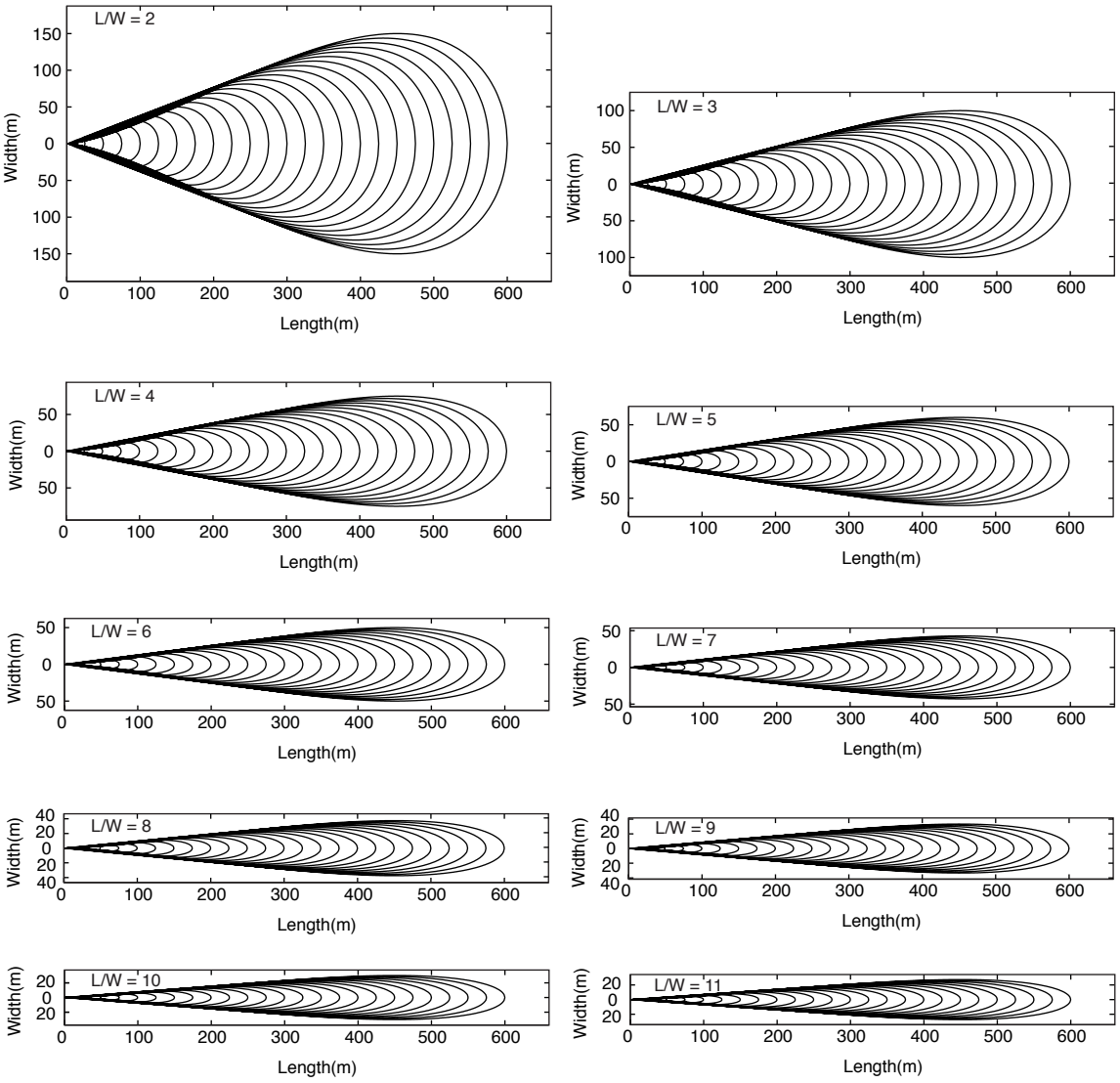

Fig. 14.—Idealized lithoherm shape based on the equation of a piriform per given length to width ratio.

where A is equal to length and B is a width based scaling factor. The equation allows the shape and area of a piriform to be determined based on a given length and maximum width (Fig. 14).

We applied this equation to model the shape of idealized lithoherms, calculating the footprint area versus length for a series of length to width ratios. Values of area and length used in this model are reflective of those observed in the actual lithoherms in our study area. When the measured data are compared with the model predictions, it is apparent that the areas of lithoherms, particularly those classified as singular, vary in an overall manner that is predictable based on their ratio of length to width (Fig. 15). There is a great deal of variation in the length to width ratio of singular lithoherms below approximately 100 m in length and 2000 m^2 in area; however, the majority of these features have a length to width ratio of 5 or less. In contrast, all but 3 of the singular lithoherms that are longer than 100 m length and have an area greater than 2000 m^2 maintain a length to width ratio between 5 and 11. This difference suggests that as singular lithoherms grow over time, they reach a threshold length and area beyond which they become more streamlined.

The orientation of individual lithoherms (Fig. 16), along with the dominantly streamlined morphology suggests that a strong unidirectional current shapes these features. Specifically, boundary layer separation likely occurs at the head of the mound, inducing a free shear layer, and the subsequent formation of an eddy along the lee of the mound before the boundary layer reattaches to the substrate. This is a negative feedback

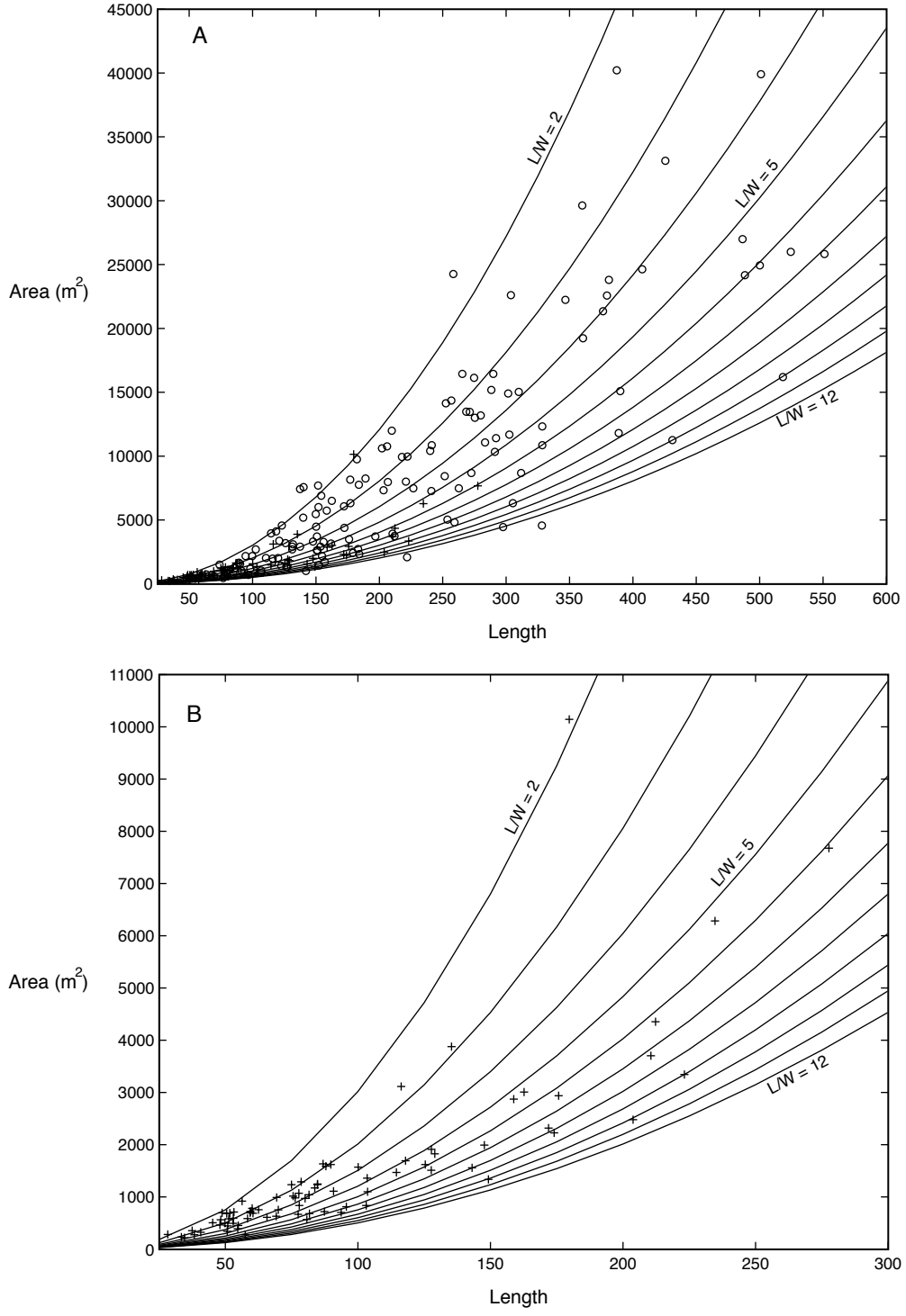

Fig. 15.—Area versus length model per given length to width ratio with actual lithoherm morphometric data superimposed. A) All data superimposed (singular and fused lithoherms). B) Enlarged view of just singular lithoherm data superimposed.

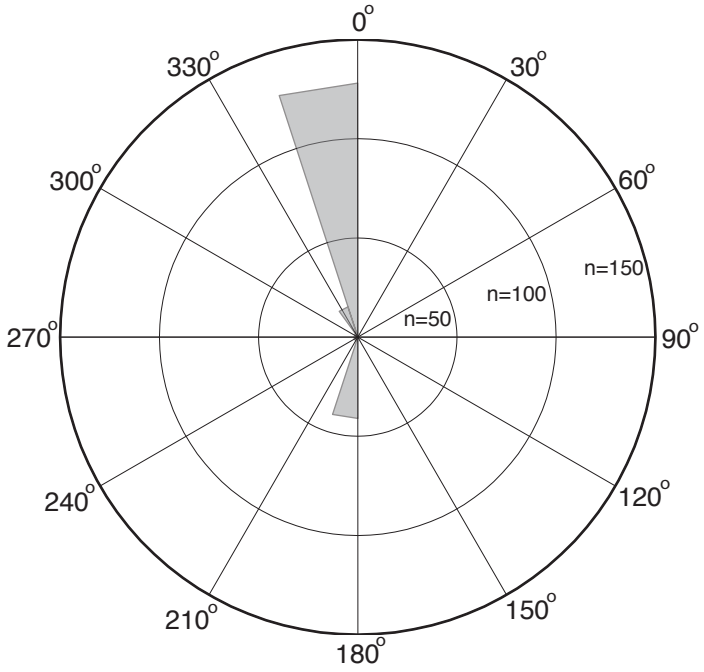

Fig. 16.—Compass plot of lithoherm long axis bearing as measured from head to tail. N = number of lithoherms.

mechanism, because the more streamlined the mound becomes, the less boundary layer separation occurs (Stanley and Swift 1976). These conclusions are supported by the current direction and speed as measured by sensors onboard the NR-1. Measurements logged at approximately one second intervals unambiguously show that during the 18.5 hours over which the survey occurred, the current azimuth bearing was consistent at approximately 350° (Fig. 17). There is some drift about this mean (300° - 30°) as a result of localized current interactions with the seafloor topography as the submarine moved through the survey area. Current intensity measurements made via the NR-1s Doppler velocity logger (DVL) did show about a 0.5 knot bias based on whether the submarine was traveling with or against the current along adjacent survey lines. However, the data do reveal a slowly undulating current velocity of approximately 0.7 knots to 0.9 knots over the course of the survey (Fig. 18). The presence of a strong unidirectional current is consistent with the findings of other studies conducted north of the Providence Channel proximal to the survey area (Leaman and Molinari 1987). Grasmueck et al. (2006) did note a contrasting scenario of tidally induced current reversals associated with mound formation along the base of Great Bahama Bank. However, this area lies approximately 300 km to the south of the lithoherm survey area where tidal reversals have been observed to occur as a result of southward flow from the Providence Channel (Gardner et al. 1989). The mounds observed by Grasmueck et al. (2006) also do not display the streamlined, piriform morphology of the lithoherms addressed in this study.

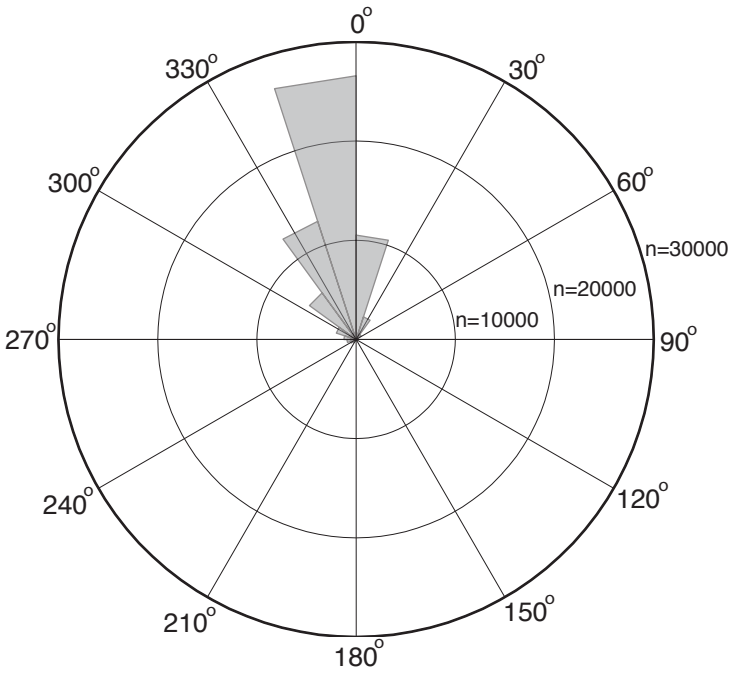

Fig. 17.—Compass plot of current bearing measured during the 18.5 hour survey. N = number of measurements (at approximately 1 second intervals) taken during the course of the survey.

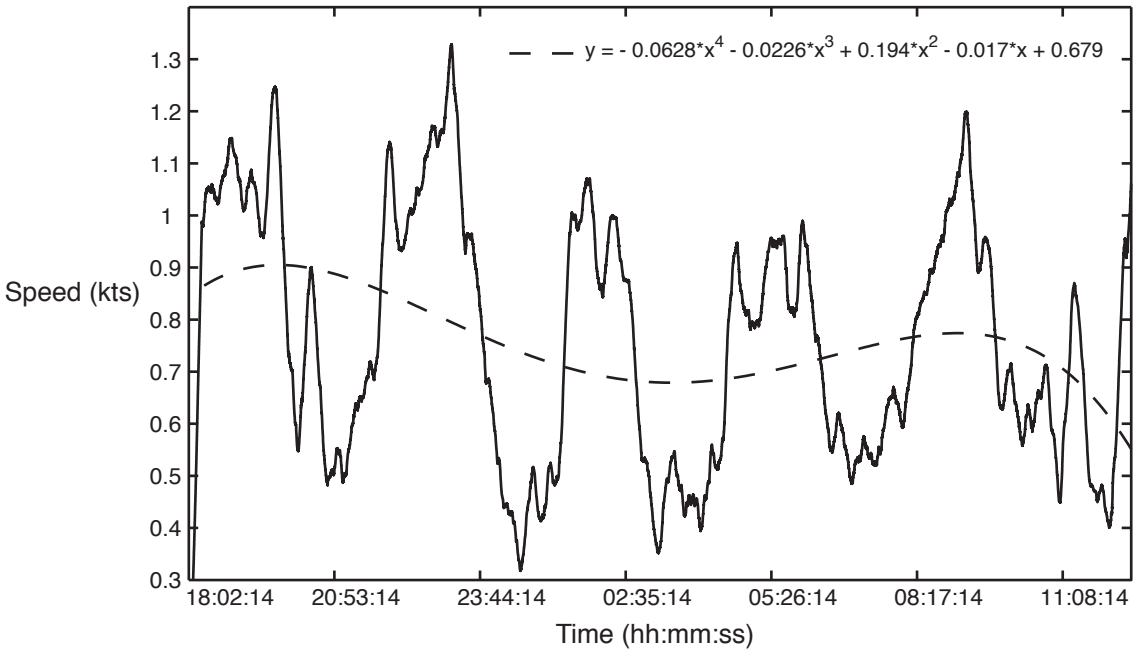

Fig. 18.—Current speed smoothed over 15 minute intervals (measured at 1 second intervals) measured during the 18.5 hour survey. A 4th order polynomial regression is fitted to the data to account for the 0.5 knot bias introduced as a result of whether the submarine was traveling with, or against the current.

Approximately 20% of the lithoherms do display a head to tail orientation that is essentially 145º to 180º opposite that of the current. Spatial investigation reveals that there is no pattern to the distribution of these features, and that they occur at random throughout the survey area. This apparently reversed orientation could result from mis-identification of the head and tail ends. It may be difficult to distinguish the head and tail ends in at least two circumstances: when a large lithoherm forms via the coalescence of smaller features, and when erosional processes degrade the head of the feature, potentially indicating a dead or dying lithoherm. Paul *et al.* (2000) discuss a complex of "transverse lithoherms" with a fluted 'saw bladed-like' pattern parallel to the current, and a long axis perpendicular to the current. We would suggest that these complex lithoherms are the result of transverse accretion of individual mounds that originally had a long axis parallel to the current.

Actual pixel resolution for the side-scan sonar data collected during the survey is approximately 0.5 m. However, due to the variation in the altitude of the submarine from the bottom, this number varies most likely between about 0.2 and 0.6 m. This resolution is not great enough for us to definitely identify individual features as may be associated with the biologic zonation model of Messing et al. (Messing et al. 1990). However, subtle variations in the character of the images do provide some very interesting clues. For instance, the mottled character of the crests of some of the mounds suggests biologic coverage. This observation is reinforced by the jagged outline of the sound shadow corresponding to the crest of the mound (Fig. 19). This observation would be consistent with the "zoanthid" zone along the crest of the idealized mound

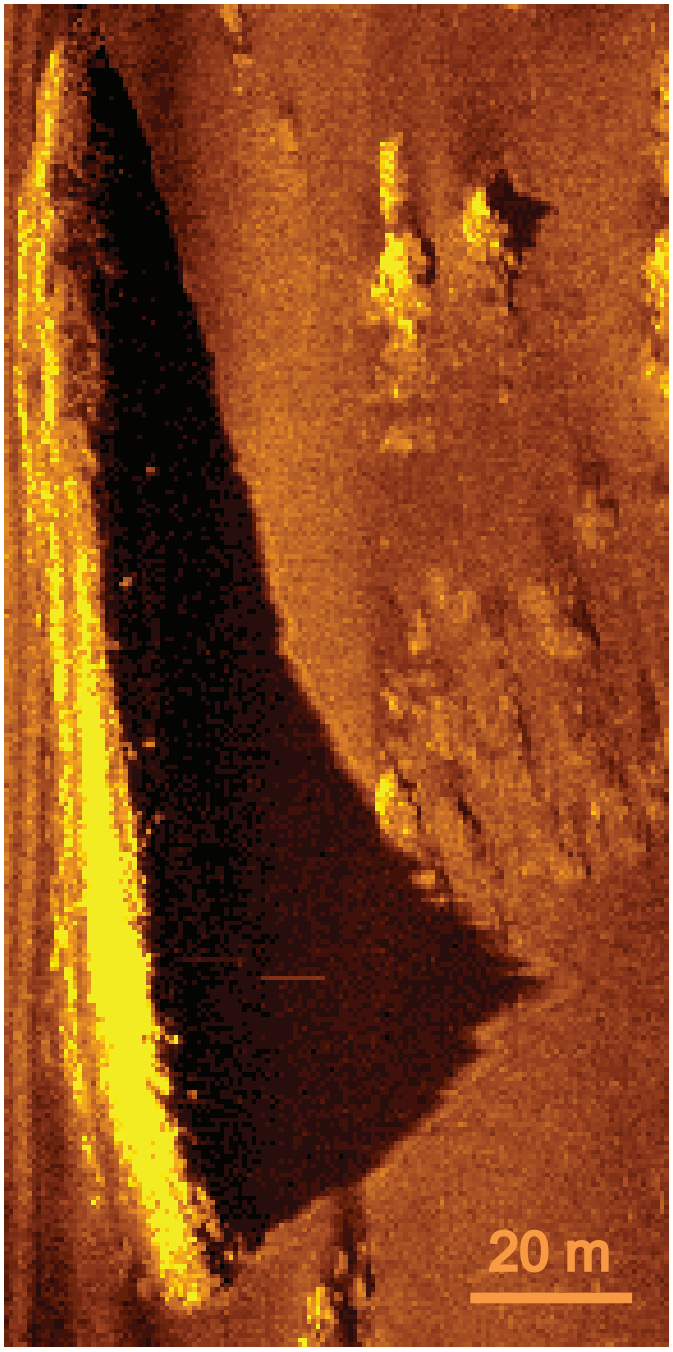

Fig. 19.—Lithoherm image showing a mottled character along the crest of the mound, and the associated jagged sound shadow.

(Messing et al. 1990). One would expect the large sea fan-like bilateral zoanthids in this zone to create a more irregular return and shadow pattern. The side-scan sonar images also reveal what appear to be ripple marks located between adjacent mounds suggesting a channelized and intensified flow (Fig. 20).

CONCLUSIONS

A side-scan sonar mounted on a submersible was used to image an 11 km^2 area of the seafloor in Straits of Florida in 650 m of water. Over two hundred individual lithoherms were identified and aspects of their morphologies were characterized, including length, width, area, height, and orientation. The lithoherms occur in greater abundance and a denser configuration than indicated by previous data. While they exhibit a range of morphologic characteristics, the lithoherms occur as either singular features or coalescent (fused) mounds. The shapes of the singular lithoherms are described well by a piriform function with varying length to width ratio. When applied to the piriform model, the data indicate that as singular lithoherms grow, they become more streamlined. Nearly all of the lithoherms are oriented with their long axis parallel to Little Bahama Bank, so their heads face directly into the Florida Current. Lithoherm morphology, along with current bearing and intensity measurements recorded while on site, confirm the dominant role the (local) strong unidirectional current plays in lithoherm formation. The results of this study contribute to better understand the nature of the lithoherms and other similar deep-water coral reefs, as well as provide a set of

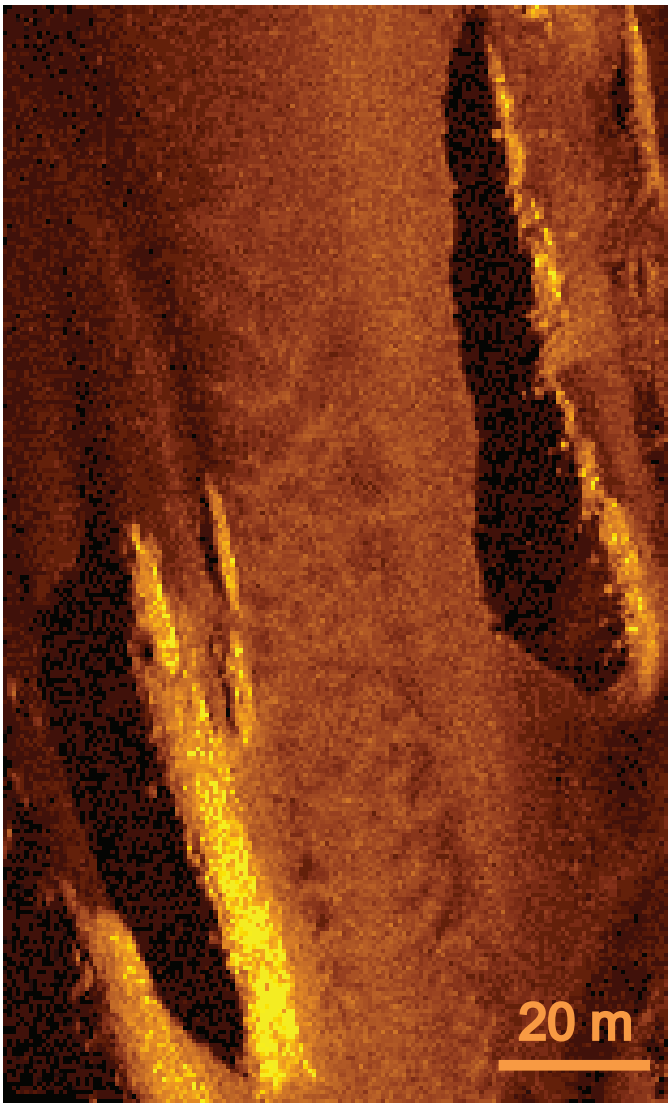

Fig. 20.—Ripple marks between adjacent lithoherms suggesting channelized flow.

constraints useful in the recognition and study of ancient coral communities and carbonate mound deposits.

CHAPTER IV

OBSERVATIONS ON THE INITIATION AND DEVELOPMENT OF THE LITHOHERM TYPE OF DEEP-WATER CORAL MOUNDS

INTRODUCTION

Lithoherms, or partially cemented deep-water coral mounds, form in much the same manner as their shallow water, light dependent, equivalent. And, as Darwin so eloquently summated, the organisms that form, colonize and destroy are "all adapted to the stations they occupy, and hold their places, like other organic beings, by a struggle one with another, and with external nature" (Darwin 1842). The initiation and sustained development of lithoherms, though not dependent on light, can be attributed to both independent environmental factors and the complex interactions of sessile organisms.

Two dominant factors must be present for lithoherm initiation and development. The first factor is the necessary seawater chemistry for the formation of hard substrates, and the continued micritic cementation of debris baffled by the coral growths on the leading edges and crests of the mounds (Paull et al. 2000; Wilber and Neumann 1993). The second factor is the persistence of a unidirectional, strong current such as The Florida Current (Hamilton et al. 2005; Leaman et al. 1987). Together, these factors produce the optimal conditions for the colonization of *Lophelia* ahermatypic scleractinean corals, sea fan like zoanthids, crinoids, sponges and a myriad of other constructive and destructive organisms (Messing et al. 1990; Messing et al. 2008; Reed et al. 2006).

The idea of categorizing deep-water coral proliferation is not a new one. In fact, the progression from colony, to thicket, to coppice, to bank has long since been inferred from the fossil record (Squires 1964). This theoretical model has been hypothetically applied to occurrences of modern deep-water coral mounds in two ways: faunal succession and mound stratigraphic development (de Haas et al. 2009; Eisele et al. 2008; Mienis et al. 2006; Mullins et al. 1981), and overall mound morphology resultant from coral proliferation about pre-existing structures such as pock marks or fluid flow features (Kenyon et al. 2003; Wheeler et al. 2008). While these examples do provide valuable insights into deep-water coral mound initiation and development, they are less than clear-cut. Here we present a qualitative model derived from direct observations and side-scan sonar imagery from a finite area (10.92 km^2) along the northwestern slope of Little Bahama Bank. In a fashion analogous to Darwin's (1842) consideration of coral atolls, we take the varied morphologies of individual lithoherms observed today to patently illustrate how lithoherms develop through time from nucleation to maturation. The purpose of this model is not to confirm previous ideas of coral succession on the local scale, but to introduce a new terminology of lithoherm development that focuses on the progression of mound morphologies. We also present a spatial analysis of lithoherm occurrence in relation to local bathymetry for the purpose of clarifying pre-existing ideas relating to the controls of the spatial distribution of these mounds.

METHODS

Over 200 individual lithoherms found in a 10.92 km^2 area in ~650 m water west of Little Bahama Bank (NW corner: 27.3295º N, 79.4366º W; SE corner: 27.2957º N, 79.4075º W) were investigated by direct observation and side-scan sonar imagery via the US Navy's *NR-1* submarine. Side-scan sonar files were examined using SeaScan PC review, and mosaiced using SonarWeb. The mosaic, as well as individual side-scan sonar files, were then exported from SonarWeb as geo-referenced image files and assessed in Global Mapper and AutoCAD. The direct observations made while onboard the submarine, along with the critical examination of the side-scan sonar imagery, provide the basis for the qualitative model presented here. A quantitative interpretation and analysis of the side-scan sonar imagery is presented elsewhere (Brookshire and Slowey in review).

Single beam echosounder data were also collected during the side-scan sonar survey. These data were gridded in Surfer using a kriging method at approximately 42 m bin spacing. The grid was smoothed via a 5 node moving average to minimize the over-expression of individual mounds lying directly within the path of the submarine. This grid was then used to create a 3d surface model of the bathymetry in Global Mapper.

RESULTS AND DISCUSSION

The initiation or nucleation of a lithoherm results from the attachment and growth of an individual colony of sessile organisms, usually *Lophelia* corals, on cemented hardgrounds (Figs. 21 & 22). The initial nucleating colony spawns additional colonies,

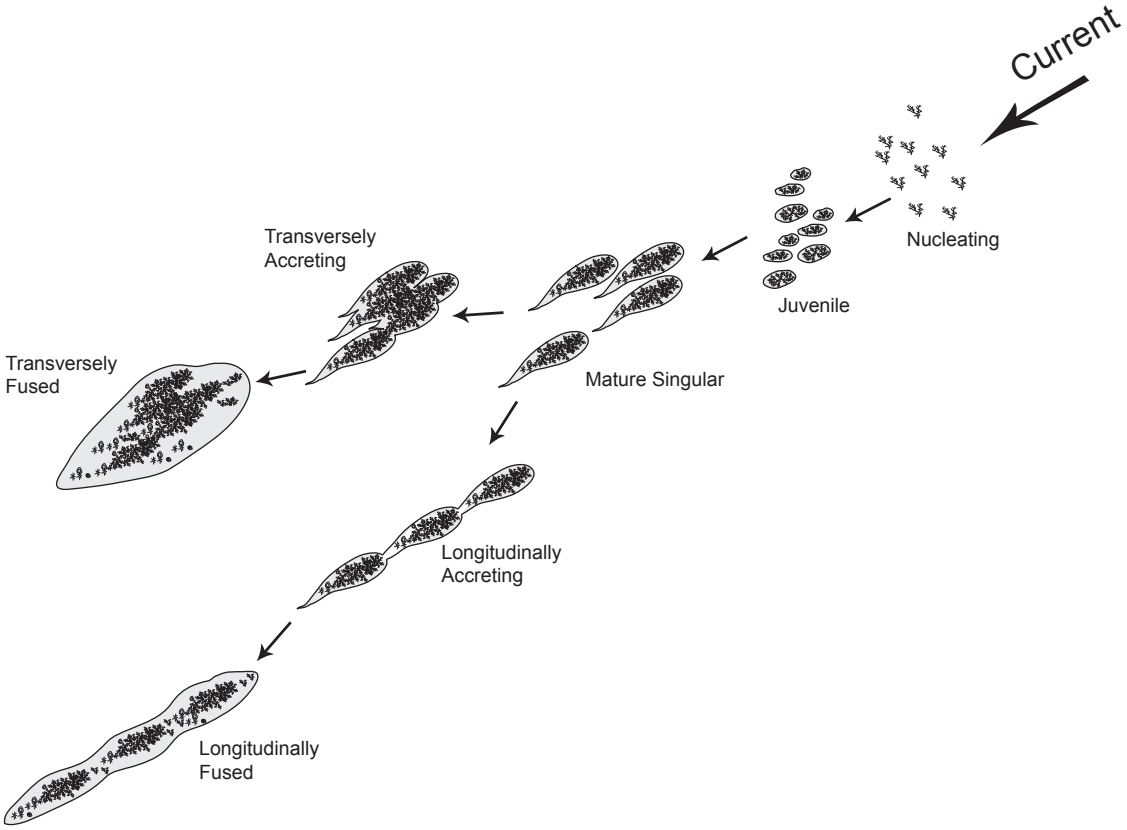

Fig 21.—Schematic drawing elucidating lithoherm development from nucleation to maturation.

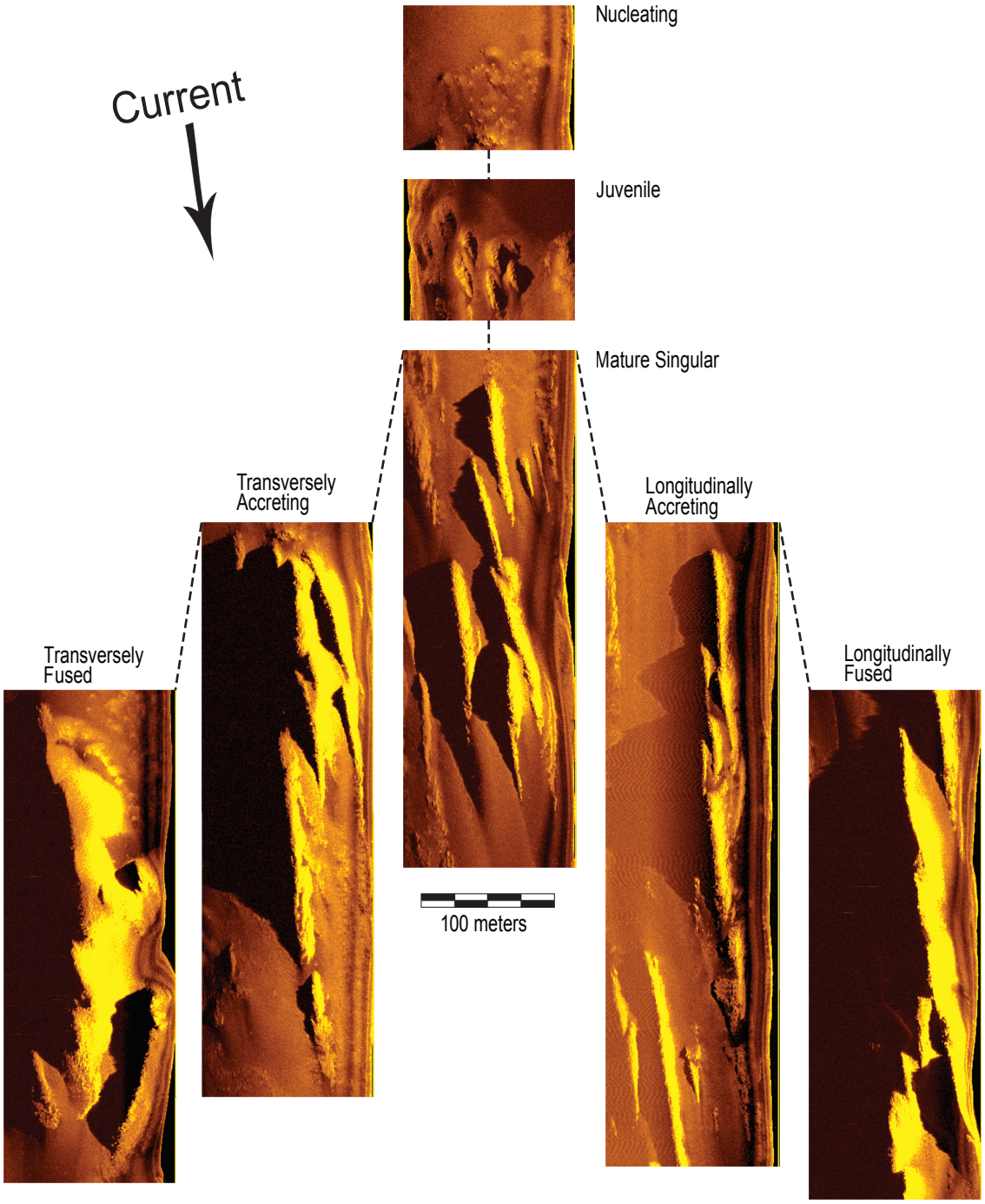

Fig 22.—Side-scan sonar data illustrating lithoherm development from nucleation to maturation.

and sediment begins to aggregate at the base of the faunal thickets as a result of their baffling effect (Messing et al. 2008; Squires 1964 among others). At this initial juvenile lithoherm stage, the small mound is relatively amorphous, but beginning to demonstrate an elongation into the current, which at our study site has a mean bearing of ~350° and mean velocity of ~40 cm sec^{-1} (Figs. 21 & 22) (Brookshire and Slowey in review). This progression has also been noted along the Rockall Trough in the northeast Atlantic where similar cold water coral "banks" originate as a result of coral colonization in pockmarks (e.g., Wheeler et al. 2008). As cementation begins to occur, and the upcurrent periphery of the juvenile lithoherm becomes suitable for attachment, colonies of *Lophelia* begin to form along the leading edge. These areas are those with the clearest window into the current, and hence the vital seston it delivers. As coral rubble accumulates at the head of the mound, creating additional area for attachment, the coral colonies advance forward into the current in a self-sustaining crawl (Messing et al. 1990). Other debris delivered by the current via saltation and traction also accumulates along the flanks and in the lee of the mound (Neumann et al. 1977). The lower flank and tail of the mound provide a substrate for filter feeding, potentially destructive, organisms such as sponges and boring mollusks (Freiwald and Wilson 1998; Messing et al. 1990). The mature singular lithoherms have an easily recognizable piriform shape as a result of this continued cycle of growth at the head, and winnowing/elongation at the tail (Brookshire and Slowey in review) (Figs. 21 & 22).

Multiple lithoherms often nucleate in close proximity as a result of localized conditions favorable to initial colonization by *Lophelia* (Reed et al. 2006) (Figs. 21 &

22). As the mature singular lithoherms continue to grow, they interact with surrounding mounds in two basic ways. Multiple lithoherms can grow into one another as a result of transverse accretion, or they can grow into one another by longitudinal accretion. In the case of transverse accretion, the heads of one or more mature lithoherms accrete into one another as a result of coral growth along the flank of the mound (Figs. 21 & 22). As transversely-fused lithoherms, individual mound crests, and multiple tails are still discernible. Over time, the combined effects of continued coral growth, the subsequent biozonation of other organisms, and the continued influence of the currents increase the uniformity of the lithoherm shape. These mature, transversely-fused lithoherms often have a much lower length to width ratio than a singular lithoherm, and have a less evident head and tail (Figs. 21 & 22). In the case of longitudinal accretion, the head of one lithoherm grows into the tail of an adjacent lithoherm (and vise versa). The longitudinally-fused lithoherm has multiple, very distinct, crests. With time, the gaps between the crests begin to close, but the majority of these mounds maintain an undulating profile. Mature longitudinally-fused lithoherms are not as distinguishable from singular lithoherms based on length to width ratio, but they have a more longitudinally symmetrical, ridge-like appearance (Figs. 21 & 22).

Certainly, fused lithoherms can form as a combined result of both transverse and longitudinal accretion. However, transverse accretion between the heads of multiple lithoherms is likely a more efficient mechanism by which fused lithoherms form. *Lophelia* can actively suppress the growth of competitive organisms by increased mucus production (Freiwald and Wilson 1998). Therefore, the *Lophelia* dominated heads of

adjacent lithoherms would fuse much more rapidly than the biologically contrasted head and tail (Freiwald and Wilson 1998). In fact, multiple lithoherms oriented perpendicular to the strike of a bathymetric high will sometimes fuse transversely along the crests in what has been described as a 'saw blade-like' pattern (Paull et al. 2000).

Comparison of the spatial occurrence of the lithoherms to the local bathymetry reveals that groups of lithoherms form in greater density along bathymetric highs (Fig. 23). The periodicity of these highs is approximately 800 m. Preliminary assessment of the orientation of the highs to the unidirectional current implies that they may be partially lithified/relict sand waves. However, two lines of evidence suggest that this is not the case. First, observed sand waves at similar depths further to the south in the Straits of Florida have a periodicity which is more than a factor of ten less than the periodicity of the bathymetric highs observed in the lithoherm study area (Gardner et al. 1989). Second, laboratory flume experiments imply that a unidirectional current velocity of 40 cm sec^{-1} is not sufficient to produce the periodicity and amplitude (~15 m) of the bathymetric highs observed in the lithoherm study area (Boguchwal and Southard 1990; Southard and Boguchwal 1990). This begs the question: are the lithoherms on top of pre-existing bathymetric highs, or are the bathymetric highs an ostensible expression of the lithoherms themselves that result from the limited resolution of the single beam echosounder? The obvious linear grouping of the lithoherms suggests that there is some contributing factor at play. A plausible explanation is that the lithoherms are forming along the levies of density flow scour channels diverging along the toe of the slope (-0.6°) (Anselmetti et al. 2000; Mullins and Neumann 1979; Wilber et al. 1993; Wilson

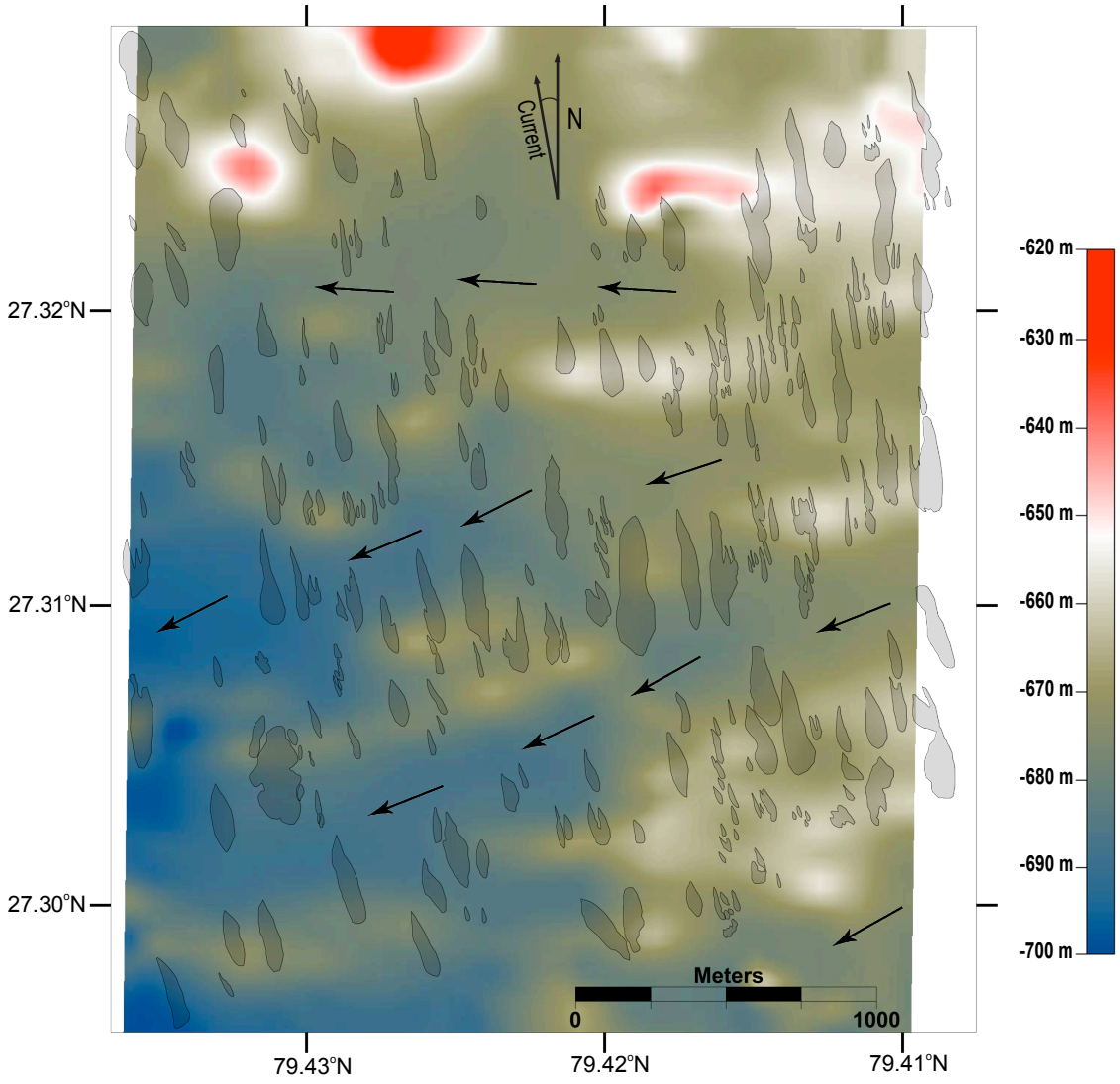

Fig. 23.—Three dimensional depth model with lithoherm footprints overlain. Arrows indicate density flow direction along scour channels.

and Roberts 1992; Wilson and Roberts 1993; Wilson and Roberts 1995). This same scenario of deep-water coral mound formation along levied channel margins at similar depths (~600-800 m) has been observed further to the south in the Straits of Florida (Grasmueck et al. 2006) and along the Rockall Trough (Mienis et al. 2006). Since the lithoherms found within the survey area do not occur exclusively along these levied channel margins, and are also found in limited number within the scour channels, we believe that the scour channels are predominantly inactive. We note that the local topographic variability could also originate in another fashion, for example, the highs could be depositional lobes of stiff, erosion-resistant sediment derived from further up the slope by mass wasting. Whether or not this is so, the same environmental conditions that favor mound development would exist and the same pattern of mound formation would result.

CONCLUSIONS AND IMPLICATIONS

Lithoherms are dynamic seabed features that form as a result of the complex interaction of a unique ecosystem with the surrounding environment. These features grow in a generally predictable pattern from the original nucleation of a sessile organism on a coarse or cemented carbonate substrate, to the mature singular or large fused lithoherm. While these features have been described as erosional or dying is some cases (Neumann et al. 1977), our evidence clearly suggests that lithoherms are actively growing in the Straits of Florida. Differential erosion and accretion are likely occurring simultaneously as opposing mechanisms necessary in the development of this unique

facies. A comparison of lithoherm spatial relationship to local bathymetry agrees with previous observations of deep-water coral mound formations along the levied margins of density flow scour channels.

CHAPTER V

CONCLUSION

Our results indicate the presence of a strong vertical gradient in $\delta^{13}C$ during the Younger Dryas cooling event. The data suggest that NAIW export to the south Atlantic may have been more reduced during the Younger Dryas than during the LGM. However, inherent $\delta^{13}C$ variability and or increased production of AAIW likely exerted dominant control of the sharp nutrient gradient. A portion of the $\delta^{13}C$ variability (0.22 $^{0}/_{00}$) can be explained by a shift in thermodynamic equilibrium concurrent with a drop in temperature of 1.8°C at the locus of Antarctic Intermediate Water (AAIW) formation (as derived from the associated $\delta^{18}O$ increase) (Mook et al. 1974). The remaining 0.37 $^{0}/_{00}$ increase in $\delta^{13}C$ most likely resulted from increased wind velocities, and a greater coupling between the ocean and the atmosphere at the locus of AAIW formation (increased efficiency of the thermodynamic process) (Ackert et al. 2008; Broecker and Maier-Reimer 1992). This wind induced variability, and subsequent increase in Eckmann induced injection of AAIW to the base of the thermocline, may help explain observed nutrient variability at low latitudes during the Younger Dryas (Ninnemann and Charles 1997; Wan et al. 2008).

A side-scan sonar mounted on a submersible was used to image an 11 km^2 area of the seafloor in Straits of Florida in 650 m of water. Over two hundred individual lithoherms were identified and aspects of their morphologies were characterized, including length, width, area, height, and orientation. The lithoherms occur in greater

abundance and a denser configuration than indicated by previous data. While they exhibit a range of morphologic characteristics, the lithoherms occur as either singular features or coalescent (fused) mounds. The shapes of the singular lithoherms are described well by a piriform function with varying length to width ratio. When applied to the piriform model, the data indicate that as singular lithoherms grow, they become more streamlined. Nearly all of the lithoherms are oriented with their long axis parallel to Little Bahama Bank, so their heads face directly into the Florida Current. Lithoherm morphology, along with current bearing and intensity measurements recorded while on site, confirm the dominant role the (local) strong unidirectional current plays in lithoherm formation. The results of this study contribute to better understand the nature of the lithoherms and other similar deep-water coral reefs, as well as provide a set of constraints useful in the recognition and study of ancient coral communities and carbonate mound deposits.

Lithoherms are dynamic seabed features that form as a result of the complex interaction of a unique ecosystem with the surrounding environment. These features grow in a generally predictable pattern from the original nucleation of a sessile organism on a coarse or cemented carbonate substrate, to the mature singular or large fused lithoherm. While these features have been described as erosional or dying is some cases (Neumann et al. 1977), our evidence clearly suggests that lithoherms are actively growing in the Straits of Florida. Differential erosion and accretion are likely occurring simultaneously as opposing mechanisms necessary in the development of this unique facies. A comparison of lithoherm spatial relationship to local bathymetry agrees with

previous observations of deep-water coral mound formations along the levied margins of density flow scour channels.

REFERENCES

Ackert, R.P., Becker, R.A., Singer, B.S., Kurz, M.D., Caffee, M.W., and Mickelson, D.M., 2008, Patagonian glacier response during the late glacial-holocene transition: Science, v. 321, p. 392-395.

Anselmetti, F.S., Eberli, G.P., and Ding, Z.D., 2000, From the Great Bahama Bank into the Straits of Florida: A margin architecture controlled by sea-level fluctuations and ocean currents: Geological Society of America Bulletin, v. 112, p. 829-844.

Armstrong, C.W., and van den Hove, S., 2008, The formation of policy for protection of cold-water coral off the coast of Norway: Marine Policy, v. 32, p. 66-73.

Bemis, B.E., Spero, H.J., Bijma, J., and Lea, D.W., 1998, Reevaluation of the oxygen isotopic composition of planktonic foraminifera: Experimental results and revised paleotemperature equations: Paleoceanography, v. 13, p. 150-160.

Bjerager, M., Surlyk, F., Lykke-Andersen, H., Thibault, N., and Stemmerik, L., 2010, Danian cool-water coral reefs in southern Scandinavia localised over seafloor highs: Marine and Petroleum Geology, v. 27, p. 455-466.

Boguchwal, L.A., and Southard, J.B., 1990, Bed configurations in steady unidirectional water flows. Part 1. Scale-model study using fine sands: Journal of Sedimentary Petrology, v. 60, p. 649-657.

Boyle, E.A., and Keigwin, L., 1987, North Atlantic thermohaline circulation during the past 20,000 years linked to high-latitude surface temperature: Nature, v. 330, p. 35-40.

Breeze, H., and Fenton, D.G., 2007, Designing management measures to protect cold-water corals off Nova Scotia, Canada, *in* George, R.Y., and Cairns, S.D., eds., Conservation and Adaptive Management of Seamount and Deep-Sea Coral Ecosystems: Miami, University of Miami, Rosenstiel School of Marine & Atmospheric Science p. 123-133.

Broecker, W.S., 2006, Was the Younger Dryas triggered by a flood?: Science, v. 312, p. 1146-1148.

Broecker, W.S., and Maier-Reimer, E., 1992, The influence of air and sea exchange on the carbon isotope distribution in the sea: Global Biogeochemical Cycles, v. 6, p. 315-320.

Broecker, W.S., and Peng, T.-S., 1982, Tracers in the Sea: Palisades, NY, Lamont-Doherty Geological Observatory.

Came, R.E., Oppo, D.W., and Curry, W.B., 2003, Atlantic Ocean circulation during the Younger Dryas: Insights from a new Cd/Ca record from the western subtropical South Atlantic: Paleoceanography, v. 18, 1086, doi: 10.1029/2003PA000888.

Charles, C.D., and Fairbanks, R.G., 1992, Evidence from Southern-Ocean sediments for the effect of North-Atlantic deep-water flux on climate: Nature, v. 355, p. 416-419.

Charles, C.D., Wright, J.D., and Fairbanks, R.G., 1993, Thermodynamic influences on the marine carbon isotope record: Paleoceanography, v. 8, p. 691-697.

Cordes, E.E., McGinley, M.P., Podowski, E.L., Becker, E.L., Lessard-Pilon, S., Viada, S.T., and Fisher, C.R., 2008, Coral communities of the deep Gulf of Mexico: Deep-Sea Research Part I-Oceanographic Research Papers, v. 55, p. 777-787.

Curry, W.B., Duplessy, J.C., and Labeyrie, L.D., 1988, Changes in the distribution of $\delta^{13}C$ of deep water ΣCO_2 between the last glaciation and the Holocene: Paleoceanography, v. 3, p. 317-341.

Darwin, C., 1842, The Structure and Distribution of Coral Reefs: The Geology of the Voyage of the Beagle: London, Smith, Elder and Co., 214 p.

de Haas, H., Mienis, F., Frank, N., Richter, T.O., Steinacher, R., de Stigter, H., van der Land, C., and van Weering, T.C.E., 2009, Morphology and sedimentology of (clustered) cold-water coral mounds at the south Rockall Trough margins, NE Atlantic Ocean: Facies, v. 55, p. 1-26.

Dolan, M.F.J., Grehan, A.J., Guinan, J.C., and Brown, C., 2008, Modelling the local distribution of cold-water corals in relation to bathymetric variables: Adding spatial context to deep-sea video data: Deep-Sea Research Part I-Oceanographic Research Papers, v. 55, p. 1564-1579.

Dorobek, S.L., and Bachtel, S.L., 2001, Supply of allochthonous sediment and its effects on development of carbonate mud mounds, Mississippian Lake Valley Formation, Sacramento Mountains, South-Central New Mexico, USA: Journal of Sedimentary Research, v. 71, p. 1003-1016.

Dorschel, B., Hebbeln, D., Foubert, A., White, M., and Wheeler, A.J., 2007, Hydrodynamics and cold-water coral facies distribution related to recent sedimentary processes at Galway Mound west of Ireland: Marine Geology, v. 244, p. 184-195.

Eisele, M., Hebbeln, D., and Wienberg, C., 2008, Growth history of a cold-water coral covered carbonate mound - Galway Mound, Porcupine Seabight, NE-Atlantic: Marine Geology, v. 253, p. 160-169.

Fairbanks, R., 1989, A 17,000-year glacio-eustatic sea level record: Influence of glacial melting rates on the Younger Dryas event and deep-ocean circulation: Nature, v. 342, p. 637-642.

Farmer, E.C., deMenocal, P.B., and Marchitto, T.M., 2005, Holocene and deglacial ocean temperature variability in the Benguela upwelling region: Implications for low-latitude atmospheric circulation: Paleoceanography, v. 20.

Feary, D.A., and James, N.P., 1998, Seismic stratigraphy and geological evolution of the Cenozoic, cool-water Eucla platform, Great Australian Bight: AAPG Bulletin-American Association of Petroleum Geologists, v. 82, p. 792-816.

Fish, J.P., and Carr, H.A., 1990, Sound Underwater Images: A Guide to the Generation and Interpretation of Side Scan Sonar Data: Orleans, MA, Lower Cape Publishing Co., 189 p.

Fosså, J.H., Mortensen, P.B., and Furevik, D.M., 2002, The deep-water coral Lophelia pertusa in Norwegian waters: Distribution and fishery impacts: Hydrobiologia, v. 471, p. 1-12.

Freiwald, A., and Wilson, J.B., 1998, Taphonomy of modern deep, cold-temperate water coral reefs: Historical Biology, v. 13, p. 37-52.

Gardner, W.D., Richardson, M.J., and Cacchione, D.A., 1989, Sedimentological effects of strong southward flow in the Straits of Florida: Marine Geology, v. 86, p. 155-180.

Grasmueck, M., Eberli, G.P., Viggiano, D.A., Correa, T., Rathwell, G., and Luo, J.G., 2006, Autonomous underwater vehicle (AUV) mapping reveals coral mound distribution, morphology, and oceanography in deep water of the Straits of Florida: Geophysical Research Letters, v. 33, p. 6.

Hamilton, P., Larsen, J.C., Leaman, K.D., Lee, T.N., and Waddell, E., 2005, Transports through the Straits of Florida: Journal of Physical Oceanography, v. 35, p. 308-322.

Heifetz, J., 2002, Coral in Alaska: Distribution, abundance, and species associations: Hydrobiologia, v. 471, p. 19-28.

Hovland, M., Vasshus, S., Indreeide, A., Austdal, L., and Nilsen, O., 2002, Mapping and imaging deep-sea coral reefs off Norway, 1982-2000: Hydrobiologia, v. 471, p. 13-17.

Johnson, H.P., and Helferty, M., 1990, The geological interpretation of side-scan sonar: Reviews of Geophysics, v. 28, p. 357-3800.

Keigwin, L.D., Jones, G.A., Lehman, S.J., and Boyle, E.A., 1991, Deglacial meltwater discharge, North-Atlantic deep circulation, and abrupt climate change: Journal of Geophysical Research-Oceans, v. 96, p. 16811-16826.

Kenyon, N.H., Akhmetzhanov, A.M., Wheeler, A.J., van Weering, T.C.E., de Haas, H., and Ivanov, M.K., 2003, Giant carbonate mud mounds in the southern Rockall Trough: Marine Geology, v. 195, p. 5-30.

Kroopnick, P.M., 1985, The distribution of 13C of ∑CO2 in the world oceans: Deep-Sea Research, v. 32, no. 1, p. 57-84.

Leaman, K.D., and Molinari, R.L., 1987, Topographic modification fo the Florida Current by Little Bahama Bank and Great Bahama Banks: Journal of Physical Oceanography, v. 17, p. 1724-1736.

Leaman, K.D., Molinari, R.L., and Vertes, P.S., 1987, Structure and Variability of the Florida Current at 27ºN: April 1982-July 1984: Journal of Physical Oceanography, v. 17, p. 565-583.

Libes, S.M., 1992, An Introduction to Marine Biogeochemistry: Toronto, John Wiley & Sons, Inc.

Marchitto, T.M., Curry, W.B., and Oppo, D.W., 1998, Millenial-scale changes in North Atlantic circulation since the last glaciation: Nature, v. 393, p. 557-561.

McManus, J.F., Francois, R., Gherardi, J.M., Keigwin, L.D., and Brown-Leger, S., 2004, Collapse and rapid resumption of Atlantic meridional circulation linked to deglacial climate changes: Nature, v. 428, p. 834-837.

Messing, C.G., Neumann, A.C., and Lang, J.C., 1990, Biozonation of deep-water lithoherms and associated hardgrounds in the Northeast Straits of Florida: Palaios, v. 5, p. 15-33.

Messing, C.G., Reed, J.K., Brook, S.D., and Ross, S.W., 2008, Deep-water coral reefs of the United States, *in* Riegl, B.M., and R.E., D., eds., Coral Reefs of the USA, Springer Science + Business Media B.V., p. 767-791.

Mienis, F., de Stigter, H.C., White, M., Dulneveldc, G., de Haas, H., and van Weering, T.C.E., 2007, Hydrodynamic controls on cold-water coral growth and carbonate-mound development at the SW and SE rockall trough margin, NE Atlantic Ocean: Deep-Sea Research Part I-Oceanographic Research Papers, v. 54, p. 1655-1674.

Mienis, F., van Weering, T., de Haas, H., de Stigter, H., Huvenne, V., and Wheeler, A., 2006, Carbonate mound development at the SW Rockall Trough margin based on high resolution TOBI and seismic recording: Marine Geology, v. 233, p. 1-19.

Miller, K., Neil, H., and Tracey, D., 2009, Recent advances in deep-sea coral science and emerging links to conservation and management of deep-sea ecosystems: Marine Ecology-Progress Series, v. 397, p. 1-5.

Mook, W.G., Bommerso.Jc, and Staverma.Wh, 1974, Carbon isotope fractionation between dissolved bicarbonate and gaseous carbon dioxide: Earth and Planetary Science Letters, v. 22, p. 169-176.

Mullins, H.T., and Neumann, A.C., 1979, Deep carbonate bank margin structure and sedimentation in the northern Bahamas: SEPM Special Publication, v. 27, p. 165-192.

Mullins, H.T., Newton, C.R., Heath, K.C., and Van Buren, H.M., 1981, Modern deep-water coral mounds north of Little Bahama Bank, criterion for recognition of deep-water coral bioherms in the rock record: Journal of Sedimentary Petrology, v. 51, p. 999-1013.

Munoz, P.D., Sayago-Gil, M., Cristobo, J., Parra, S., Serrano, A., del Rio, V.D., Patrocinio, T., Sacau, M., Murillo, F.J., Palomino, D., and Fernandez-Salas, L.M., 2009, Seabed mapping for selecting cold-water coral protection areas on Hatton Bank, Northeast Atlantic: Ices Journal of Marine Science, v. 66, p. 2013-2025.

Murillo-Muneton, G., and Dorobek, S.L., 2003, Controls on the evolution of carbonate mud mounds in the Lower Cretaceous Cupido Formation, northeastern Mexico: Journal of Sedimentary Research, v. 73, p. 869-886.

Muscheler, R., Kromer, B., Bjorck, S., Svensson, A., Friedrich, M., Kaiser, K.F., and Southon, J., 2008, Tree rings and ice cores reveal C-14 calibration uncertainties during the Younger Dryas: Nature Geoscience, v. 1, p. 263-267.

Neumann, A.C., Kofoed, J.W., and Keller, G.H., 1977, Lithoherms in the Straits of Florida: Geology, v. 5, p. 4-10.

Ninnemann, U.S., and Charles, C.D., 1997, Regional differences in Quaternary Subantarctic nutrient cycling: Link to intermediate and deep water ventilation: Paleoceanography, v. 12, p. 560-567.

O'Connor, J.J., and Robertson, E.F., 2004, Pearshaped, The MacTutor History of Mathematics Archive: St. Andrews, School of Mathematics and Statistics, University of St. Andrews Scotland.

Ostlund, H.G., Craig, H., Broecker, W., and Spencer, D., 1987, GEOSECS: Atlantic, Pacific, and Indian Ocean Expeditions: Shorebased Data and Graphics, v. 7: Washington DC, 20402, US Government Printing Office, 200 p.

Pahnke, K., Goldstein, S.L., and Hemming, S.R., 2008, Abrupt changes in Antarctic Intermediate Water circulation over the past 25,000 years: Nature Geoscience, v. 1, p. 870-874.

Paull, C.K., Neumann, A.C., am Ende, B.A., Ussler III, W., and Rodriguez, N.M., 2000, Lithoherms on the Florida-Hatteras slope: Marine Geology, v. 166, p. 83-101.

Pond, S., and Pickard, G.L., 1983, Introductory Dynamical Oceanography: Oxford, Butterworth-Heinemann, 329 p.

Reed, J.K., 2002, Comparison of deep-water coral reefs and lithoherms off southeastern USA: Hydrobiologia, v. 471, p. 57-69.

Reed, J.K., Koenig, C.C., and Shepard, A.N., 2007, Impacts of bottom trawling on a deep-water Oculina coral ecosystem off Florida: Bulletin of Marine Science, v. 81, p. 481-496.

Reed, J.K., Weaver, D.C., and Pomponi, S.A., 2006, Habitat and fauna of deep-water Lophelia pertusa coral reefs off the southeastern U.S.: Blake Plateau, Straits of Florida, and Gulf of Mexico: Bulletin of Marine Science, v. 78, p. 343-375.

Roark, B.E., Guilderson, T.P., Dunbar, R.B., Fallon, S.J., and Mucciarone, D.A., 2009, Extreme longevity in proteinaceous deep-sea corals: Proceedings of the National Academy of Sciences of the United States of America, v. 106, p. 5204-5208.

Romanek, C.S., Grossman, E.L., and Morse, J.W., 1992, Carbon isotopic fractionation in synthetic aragonite and calcite: Effects of temperature and precipitation rate: Geochimica et Cosmochimica Acta, v. 56, p. 419-430.

Ruggeberg, A., Fietzke, J., Liebetrau, V., Eisenhauer, A., Dullo, W.C., and Freiwald, A., 2008, Stable strontium isotopes (delta Sr-88/86) in cold-water corals - A new proxy for reconstruction of intermediate ocean water temperatures: Earth and Planetary Science Letters, v. 269, p. 569-574.

Schlitzer, R., 2004, Ocean Data View, http//:odv.awi.de/: Bremerhaven.

Schroeder, W.W., 2002, Observations of Lophelia pertusa and the surficial geology at a deep-water site in the northeastern Gulf of Mexico: Hydrobiologia, v. 471, p. 29-33.

Singarayer, J.S., Richards, D.A., Ridgwell, A., Valdes, P.J., Austin, W.E.N., and Beck, J.W., 2008, An oceanic origin for the increase of atmospheric radiocarbon during the Younger Dryas: Geophysical Research Letters, v. 35, L14707, doi: 10.1029/2008GL034074.

Slowey, N., and Curry, W.B., 1995, Glacial-interglacial differences in circulation and carbon cycling within the upper western North Atlantic: Paleoceanography, v. 10, p. 715-732.

Southard, J.B., and Boguchwal, L.A., 1990, Bed configurations in steady unidirectional water flows. Part 2. Synthesis of flume data: Journal of Sedimentary Petrology, v. 60, p. 658-679.

Squires, D.F., 1964, Fossil coral thickets in Wairarapa, New Zealand: Journal of Paleontology, v. 38, p. 904-915.

Stanley, D.J., and Swift, D.J.P., 1976, Marine Sediment Transport and Environmental Management: New York, John Wiley & Sons, p. 602.

Stuiver, M., and Reimer, P., 1986-2005, CALIB: http//:calib.qub.ac.uk/calib/.

Stuiver, M., and Reimer, P., 2009, Marine Reservoir Correction Database: http//:calib.qub.ac.uk/marine/.

Sverdrup, H.U., Johnson, M.W., and Fleming, R.H., 1942, The Oceans: Their Physics, Chemistry, and General Biology: Englewood Cliffs, NJ, Prentice-Hall, 1087 p.

Titschack, J., and Freiwald, A., 2005, Growth, deposition, and facies of Pleistocene bathyal coral communities from Rhodes, Greece, *in* Freiwald, A., and Roberts, J.M., eds., Cold-water Corals and Ecosystems: Berlin Heidelberg, Springer-Verlag, p. 41-59.

Trabant, P.K., 1984, Applied High-resolution Geophysical Methods: Offshore Geoengineering Hazards, International Human Resources Development Corp., 265 p.

van Weering, T.C.E., de Haas, H., de Stigter, H.C., Lykke-Anderson, H., and Kouvaev, I., 2003, Structure and development of giant carbonate mounds at the SW and SE Rockall Trough margins, NE Atlantic Ocean: Marine Geology, v. 313, p. 1-15.

Wan, X., Chang, P., Saravanan, R., Zhang, R., and Schmidt, M.W., 2008, On the interpretation of Caribbean paleo-temperature reconstructions during the Younger Dryas: Geophysical Research Letters, v. 35.

Wheeler, A.J., Kozachenko, M., Masson, D.G., and Huvenne, V.A.I., 2008, Influence of benthic sediment transport on cold-water coral bank morphology and growth: The example of the Darwin Mounds, north-east Atlantic: Sedimentology, v. 55, p. 1875-1887.

Wilber, J.R., and Neumann, A.C., 1993, Effects of submarine cementation on microfabrics and physical properties of carbnate slope deposits, Northern Bahamas, *in* Rezak, R., and Lavoie, D.L., eds., Carbonate Microfabrics: New York, Springer, p. 79-94.

Wilber, R.J., Whitehead, J., Halley, R.B., and Milliman, J.D., 1993, Carbonate-periplatform sedimentation by density flows: A mechanism for rapid off-bank and vertical transport of shallow-water fines: Comment: Geology, v. 21, p. 667-668.

Wilson, P.A., and Roberts, H.H., 1992, Carbonate-periplatform sedimentation by density flows: A mechanism for rapid off-bank and vertical transport of shallow-water fines: Geology, v. 20, p. 713-716.

Wilson, P.A., and Roberts, H.H., 1993, Carbonate-periplatform sedimentation by density flows: A mechanism for rapid off-bank and vertical transport of shallow-water fines: Reply: Geology, v. 21, p. 668-669.

Wilson, P.A., and Roberts, H.H., 1995, Density cascading: Off-shelf sediment transport, evidence and implications, Bahama Banks: Journal of Sedimentary Research Section a-Sedimentary Petrology and Processes, v. 65, p. 45-56.

VITA

Name: Brian Neville Brookshire Jr.

Address: C/O Niall Slowey
Texas A&M University
O&M Building, Room 316
MS 3146
College Station, Texas 77843

Email Address: bnbrookshire@gmail.com

Education: Ph.D., Oceanography, Texas A&M University, 2010

M.S., Oceanography, Texas A&M University, 2003

B.S., Marine Science, Eckerd College, 1999